

# m<sup>6</sup>A RNA methylation orchestrates transcriptional dormancy during paused pluripotency

Received: 7 July 2022

Accepted: 21 July 2023

Published online: 7 September 2023

 Check for updates

Evelyne Collignon<sup>1,4</sup>✉, Brandon Cho<sup>1</sup>, Giacomo Furlan<sup>1</sup>, Julie Fothergill-Robinson<sup>1</sup>, Sylvia-Bryn Martin<sup>1</sup>, Sarah A. McClymont<sup>1</sup>, Robert L. Ross<sup>2</sup>, Patrick A. Limbach<sup>3</sup> & Miguel Ramalho-Santos<sup>1</sup>✉

Embryos across metazoan lineages can enter reversible states of developmental pausing, or diapause, in response to adverse environmental conditions. The molecular mechanisms that underlie this remarkable dormant state remain largely unknown. Here we show that N<sup>6</sup>-methyladenosine (m<sup>6</sup>A) RNA methylation by *Mettl3* is required for developmental pausing in mouse blastocysts and embryonic stem (ES) cells. *Mettl3* enforces transcriptional dormancy through two interconnected mechanisms: (1) it promotes global mRNA destabilization and (2) it suppresses global nascent transcription by destabilizing the mRNA of the transcriptional amplifier and oncogene *N-Myc*, which we identify as a crucial anti-pausing factor. Knockdown of *N-Myc* rescues pausing in *Mettl3*<sup>-/-</sup> ES cells, and forced demethylation and stabilization of *Mycn* mRNA in paused wild-type ES cells largely recapitulates the transcriptional defects of *Mettl3*<sup>-/-</sup> ES cells. These findings uncover *Mettl3* as a key orchestrator of the crosstalk between transcriptomic and epitranscriptomic regulation during developmental pausing, with implications for dormancy in adult stem cells and cancer.

Development is often assumed to be a sequential unfolding of genetic programmes towards increased complexity and occurring with stereotypical timing. However, adjusting developmental timing can enhance survival in adverse conditions<sup>1,2</sup>. In mammals, this manifests as embryonic diapause, the delayed implantation of the blastocyst<sup>3,4</sup>. The switch to a dormant state of paused pluripotency can be induced in mouse blastocysts and ES cells through the inhibition of mTOR, a conserved growth-promoting kinase, and is characterized by a substantial global decrease in biosynthetic activity, including gene transcription<sup>5</sup>. Global inhibition of translation<sup>6</sup> or of *Myc* transcription factors<sup>7</sup> can capture features of ES cell pausing but, unlike mTOR inhibition, does

not recapitulate blastocyst diapause<sup>5</sup>. How the transcriptionally dormant state, or hypotranscription, of paused ES cells and blastocysts is induced remains poorly understood.

RNA modifications have recently emerged as a key layer of regulation of the transcriptome. m<sup>6</sup>A is the most abundant and best understood of all known mRNA modifications<sup>8</sup>. The methyl group is deposited on nascent RNA by a methyltransferase complex, with *Mettl3* as the catalytically active subunit<sup>9,10</sup>. The mark plays essential roles during post-implantation development through mRNA destabilization of key cell fate regulators, including *Klf4*, *Nanog* and *Sox2* (refs. 11–13). In mouse ES cells, the m<sup>6</sup>A readers Ythdf1–Ythdf3 promote

<sup>1</sup>Lunenfeld–Tanenbaum Research Institute and Department of Molecular Genetics, University of Toronto, Toronto, Ontario, Canada. <sup>2</sup>Thermo Fisher Scientific, Franklin, MA, USA. <sup>3</sup>Rieveschl Laboratories for Mass Spectrometry, Department of Chemistry, University of Cincinnati, Cincinnati, OH, USA.

<sup>4</sup>Present address: Laboratory of Cancer Epigenetics, Faculty of Medicine, ULB-Cancer Research Centre (U-CRC) and Institut Jules Bordet, Université Libre de Bruxelles, Brussels, Belgium. ✉e-mail: [evelyne.collignon@ulb.be](mailto:evelyne.collignon@ulb.be); [mrsantos@lunenfeld.ca](mailto:mrsantos@lunenfeld.ca)

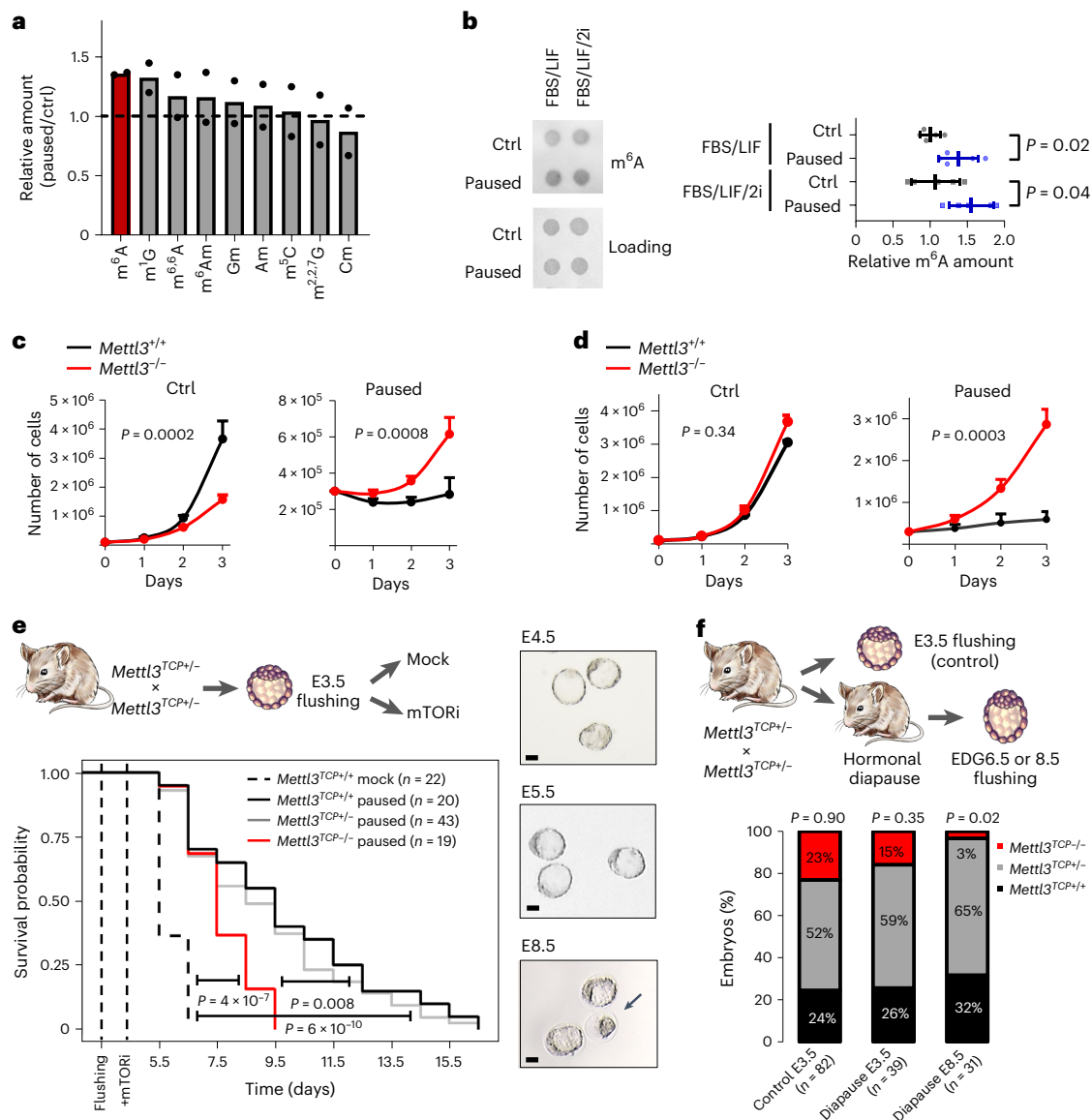


**Fig. 1 | The m<sup>6</sup>A methyltransferase *Mettl3* is essential for paused pluripotency.** **a**, Screening of RNA modifications by mass spectrometry in poly(A) RNA. Levels in paused ES cells are normalized to control (ctrl) ES cells. Data are the mean,  $n = 2$  biological replicates. **b**, Left, Dot blot showing an increase in m<sup>6</sup>A levels in paused ES cells in FBS/LIF or FBS/LIF/2i medium. Right, Levels of m<sup>6</sup>A are normalized to a RNA loading control (methylene blue staining). Data are the mean  $\pm$  s.d.,  $n = 5$  biological replicates. **c,d**, Growth curves showing that *Mettl3*<sup>-/-</sup> ES cells fail to suppress proliferation in paused conditions, both in media containing fetal bovine serum and leukaemia inhibitory factor (FBS/LIF) (**c**) and media supplemented with GSK3 $\beta$  and Mek1/2 inhibitors (FBS/LIF/2i) (**d**). Data are the mean  $\pm$  s.e.m.,  $n = 3$  biological replicates. **e**, Top, schematic of

experiment. Bottom, *Mettl3* loss leads to the premature death of mouse blastocysts cultured ex vivo in paused conditions. Right, Sample images of cultured embryos, with the black arrow indicating a dead embryo. Scale bar, 50  $\mu$ m. **e**, embryonic day; mTORi, mTOR inhibition. **f**, Top, Schematic of experiment. Bottom, Quantification of recovered (live) embryos at E3.5 (control) or at equivalent days of gestation (EDG) 6.5 and 8.5 following hormonal diapause showing that *Mettl3*<sup>TCP-/-</sup> embryos are impaired at undergoing hormonal diapause. Number of embryos ( $n$ ) as indicated (**e,f**).  $P$  values (as indicated on figure) by two-tailed Student's  $t$ -tests (**b**), linear regression test with interaction (**c,d**), log-rank test (**e**) or  $\chi^2$  test (**f**).

RNA decay, with possible compensation between the readers<sup>14</sup>. In addition, m<sup>6</sup>A RNA methylation was recently reported to modulate the transcriptional state of ES cells by destabilizing chromosome-associated RNAs and transposon-derived RNAs<sup>15–17</sup> and by promoting the recruitment of heterochromatin regulators<sup>18</sup>. Given these documented roles of m<sup>6</sup>A in the transcriptome of ES cells, we set out to explore a potential function of RNA modifications in the regulation of transcriptional dormancy during diapause. Our results show that *Mettl3*-mediated m<sup>6</sup>A RNA methylation is essential for mouse developmental pausing, and uncover a *Mettl3*–N-Myc mRNA axis that orchestrates transcriptional dormancy of paused cells.

## Results

### *Mettl3* is required for paused pluripotency

To investigate a potential role of RNA modifications in developmental pausing, we first performed a comprehensive screen in ES cells paused by mTOR inhibition. Mass spectrometry revealed significantly increased levels of m<sup>6</sup>A in paused ES cells relative to control conditions (Fig. 1a and Extended Data Fig. 1a). The increase in m<sup>6</sup>A was also observed by dot blot in paused ES cells that were induced by chemical inhibition of mTOR or by dual knockdown of mTORC1 and mTORC2 (Fig. 1b and Extended Data Fig. 1b–d). Paused ES cells induced by mTOR inhibition are viable and pluripotent but proliferate slower

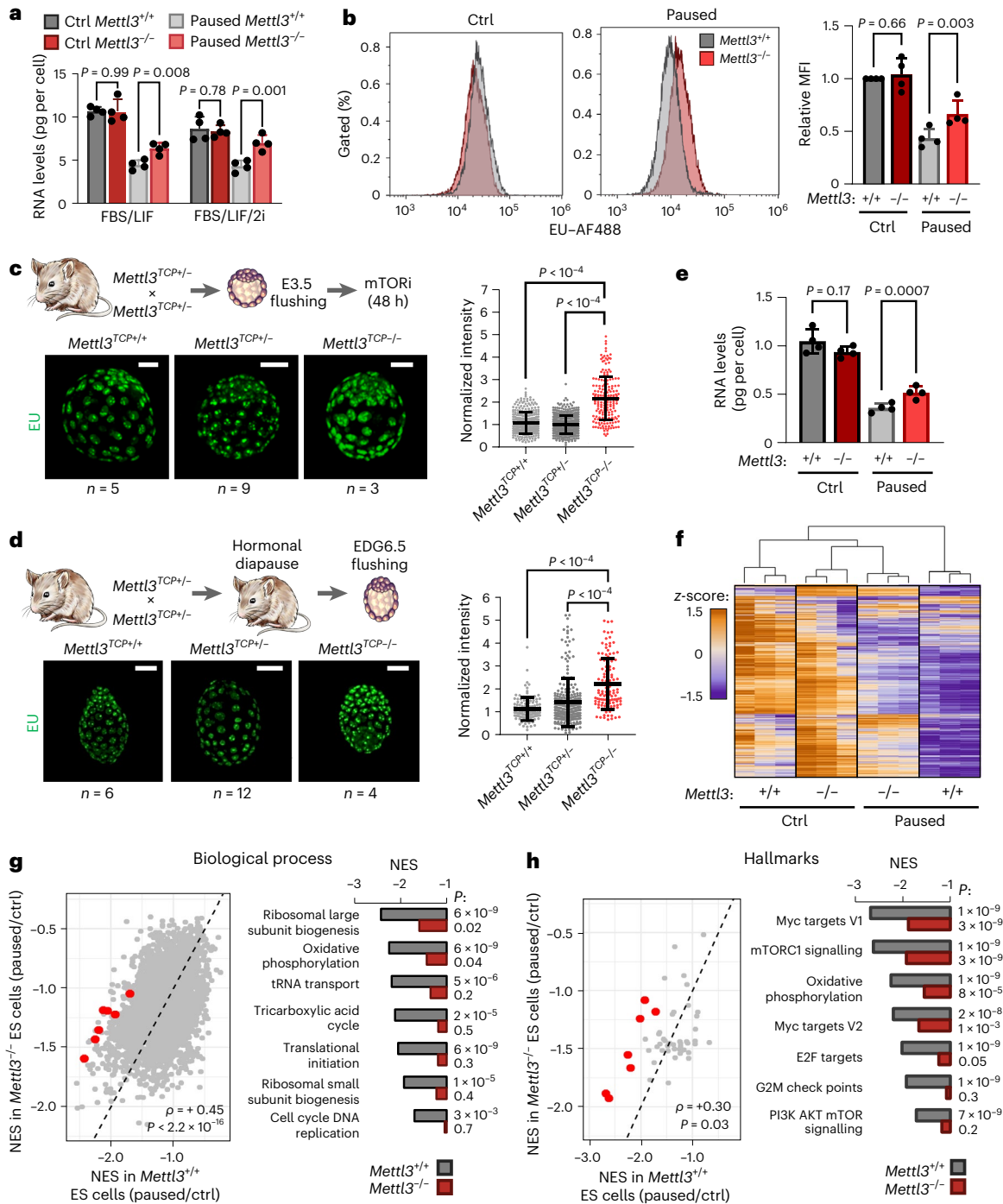


**Fig. 2 | Mettl3 regulates hypotranscription in paused pluripotency.**

**a**, Quantification of total RNA per cell in *Mettl3*<sup>+/+</sup> and *Mettl3*<sup>-/-</sup> ES cells grown in control and paused conditions in FBS/LIF or FBS/LIF/2i media. Data are the mean  $\pm$  s.d.,  $n = 4$  biological replicates. **b**, Representative histograms (left) of nascent transcription in *Mettl3*<sup>+/+</sup> and *Mettl3*<sup>-/-</sup> ES cells grown in control or paused conditions and quantification (right) by median fluorescence intensity (MFI) relative to control *Mettl3*<sup>+/+</sup> cells in each experiment, which show increased transcription in paused *Mettl3*<sup>-/-</sup> ES cells. Data are the mean  $\pm$  s.d.,  $n = 4$  biological replicates. Examples of FACS gating have been deposited into the Figshare repository (<https://doi.org/10.6084/m9.figshare.23551986>). **c,d**, Immunofluorescence images (left) and nuclear signal quantification (right) of 5-ethynyl uridine (EU) incorporation in ex vivo paused (**c**) and hormonally diapaused (**d**) blastocysts showing increased nascent transcription in *Mettl3*<sup>TCP-/-</sup> cells. Data are the mean  $\pm$  s.d. Number of embryos ( $n$ ) as indicated. Scale bar, 50  $\mu$ m. **e**, Quantification of poly(A) RNA per cell in *Mettl3*<sup>+/+</sup> and *Mettl3*<sup>-/-</sup> ES cells

grown in control and paused conditions. Data are the mean  $\pm$  s.d.,  $n = 4$  biological replicates. **f**, Heatmap of gene expression (by RNA-seq) for all genes expressed in *Mettl3*<sup>+/+</sup> and *Mettl3*<sup>-/-</sup> ES cells showing defective hypotranscription in paused *Mettl3*<sup>-/-</sup> ES cells. Data as z-score normalized per gene, with all samples displayed ( $n = 3$  biological replicates per group). **g,h**, Gene set enrichment analysis (GSEA) of gene expression changes in paused *Mettl3*<sup>+/+</sup> and *Mettl3*<sup>-/-</sup> ES cells (as shown in Fig. 2f), using the ‘GO biological processes’ (**g**) and ‘hallmarks’ collections (**h**). Scatter plots (left) of the normalized enrichment scores (NES), with Spearman’s correlation coefficient ( $\rho$ ). Representative pathways with defective hypotranscription in *Mettl3*<sup>-/-</sup> (red dots) are highlighted (right).  $P$  values (as indicated on the figure) by two-tailed paired Student’s  $t$ -tests (**a,b,e**), one-way analysis of variance (ANOVA) with Dunnett’s multiple comparison test (**c,d**) or two-sided pre-ranked GSEA with Benjamini–Hochberg false discovery rate (FDR) correction (**f,g**).

than control ES cells<sup>5</sup>. Notably, paused *Mettl3*<sup>-/-</sup> ES cells grew at a faster rate than paused wild-type (*Mettl3*<sup>+/+</sup>) ES cells, which suggested that there was defective suppression of proliferation after the loss of *Mettl3* (Fig. 1c,d and Extended Data Fig. 1e–h). Interestingly, this faster proliferation rate of *Mettl3*<sup>-/-</sup> ES cells relative to *Mettl3*<sup>+/+</sup> cells was observed only in the paused state and not in control conditions (Fig. 1c,d and Extended Data Fig. 1h), which implicates a specific role for this factor in developmental pausing. To explore a potential role of *Mettl3* in blastocyst pausing, we turned to *Mettl3*<sup>-/-</sup> mice (see model in Extended Data Fig. 1i,j). As we have previously reported, inhibition of mTOR prolongs the survival of blastocysts ex vivo for 1–2 weeks and induces a paused state<sup>5</sup>, a finding reproduced here with *Mettl3*<sup>+/+</sup> embryos (Fig. 1e). By contrast, *Mettl3*<sup>-/-</sup> blastocysts were prematurely lost during ex vivo pausing (Fig. 1e). *Mettl3*<sup>-/-</sup> embryos were also largely incompatible with hormonally induced diapause (Fig. 1f). Taken together, these findings reveal an essential role of *Mettl3* in ES cell and blastocyst pausing.

### **Mettl3 is required for transcriptional dormancy**

In light of the global hypotranscription observed in diapause<sup>5</sup>, we next explored the status of transcription in *Mettl3*<sup>-/-</sup> paused ES cells and blastocysts. In comparison to paused *Mettl3*<sup>+/+</sup> cells, paused *Mettl3*<sup>-/-</sup> ES cells display increased levels of both total and nascent RNA per cell (Fig. 2a,b and Extended Data Fig. 2a). Levels of nascent RNA were also increased in ex vivo paused and hormonally diapaused *Mettl3*<sup>-/-</sup> blastocysts compared with *Mettl3*<sup>+/+</sup> or *Mettl3*<sup>+/+</sup> embryos (Fig. 2c,d and Extended Data Fig. 2b).

Paused *Mettl3*<sup>-/-</sup> ES cells also displayed higher levels of poly(A) RNA per cell (Fig. 2e). Therefore, we performed cell-number-normalized mRNA-sequencing, which uses exogenous RNA spike-ins and enables the quantification of global shifts in transcriptional output<sup>19</sup>, in *Mettl3*<sup>+/+</sup> and *Mettl3*<sup>-/-</sup> control and paused ES cells (Extended Data Fig. 2c, Supplementary Table 1 and Methods). In line with the global changes observed in poly(A) RNA levels (Fig. 2e), paused *Mettl3*<sup>-/-</sup> ES cells displayed a defective hypotranscriptional state (Fig. 2f and Extended Data Fig. 2d–f). Indeed, whereas 10,656 genes were downregulated in paused *Mettl3*<sup>+/+</sup> cells, only 5,916 genes (that is, 55.5%) were downregulated in paused *Mettl3*<sup>-/-</sup> cells (Extended Data Fig. 2e). This suppression of hypotranscription in paused *Mettl3*<sup>-/-</sup> ES cells was particularly evident for pathways and functional categories for which silencing is a feature of developmental pausing, such as translation, ribosome biogenesis, mTOR signalling, Myc targets and energy metabolism<sup>4,5,7,20,21</sup> (Fig. 2g,h, Extended Data Fig. 2g,h and Supplementary Table 2). The kinase activity of the mTORC1 complex itself did not appear to be aberrantly activated in paused *Mettl3*<sup>-/-</sup> ES cells (Extended Data Fig. 2i). This finding suggests that the mTORC1 pathway signature depicted in Fig. 2h is driven by the overall transcriptional shift of *Mettl3*<sup>-/-</sup> ES cells towards a less paused, more proliferative state with which the mTOR pathway is often associated. Overall, these results reveal that *Mettl3* contributes to the state of global transcriptional dormancy observed during developmental pausing.

### **Mettl3 sustains dormancy through its methyltransferase activity**

To probe the mechanism by which *Mettl3* regulates pausing, we transfected *Mettl3*<sup>-/-</sup> ES cells with either wild-type *Mettl3* or a catalytically inactive mutant protein<sup>22</sup> (Fig. 3a). Only wild-type *Mettl3* rescued the ES cell pausing phenotype of *Mettl3*<sup>-/-</sup> ES cells (Fig. 3b,c), which indicated that m<sup>6</sup>A methyltransferase activity is necessary to induce paused pluripotency. Thus, we next mapped m<sup>6</sup>A modifications transcriptome-wide by methylated RNA immunoprecipitation followed by sequencing (MeRIP-seq) using a cell-number-normalization approach (Extended Data Fig. 3a–e and Methods). We identified 15,046 m<sup>6</sup>A peaks within 7,095 genes, which represents 48% of all genes expressed in control or paused ES cells (Supplementary Table 3). Principal component analysis (PCA) revealed that paused ES cells are in a distinct state with regards

to the m<sup>6</sup>A RNA profile (Fig. 3d). Consistent with the quantitative mass spectrometry analysis (Fig. 1a), MeRIP-seq showed a global increase in m<sup>6</sup>A in paused ES cells, with 1,562 peaks significantly hypermethylated compared with only 249 regions hypomethylated relative to control ES cells (Fig. 3e and Extended Data Fig. 3f–h).

To understand the gain in m<sup>6</sup>A in paused ES cells, we investigated the levels of *Mettl3* protein. Interestingly, despite no change in whole cell levels of m<sup>6</sup>A writers or erasers, *Mettl3* was greatly increased in the chromatin compartment following transition to the paused state (Extended Data Fig. 4a,b). *Mettl3* has previously been shown to bind to chromatin in normal ES cells and in cancer cells, where it deposits m<sup>6</sup>A co-transcriptionally<sup>18,23–25</sup>. We therefore mapped the genome-wide distribution of *Mettl3* by chromatin immunoprecipitation followed by sequencing (ChIP-seq) using a cell-number-normalization approach (Extended Data Fig. 4c,d and Methods). As anticipated, we observed higher levels of *Mettl3* occupancy in paused ES cells relative to control ES cells (Fig. 3f). Although *Mettl3* bound extensively throughout the genome, it was more abundant over expressed genes, particularly if their RNAs were also m<sup>6</sup>A methylated (Extended Data Fig. 4e). The majority of m<sup>6</sup>A methylated RNAs (4,922 out of 7,095, 69.4%) were transcribed from genes occupied by *Mettl3* in ES cells, and transcripts gaining m<sup>6</sup>A during pausing often arose from genes with increased *Mettl3* binding in paused ES cells (542 out of 1,616, 33.5%; Fig. 3g and Extended Data Fig. 4f). In agreement with recent reports<sup>18,23</sup>, *Mettl3* localized mainly to the transcriptional start site (TSS), whereas m<sup>6</sup>A was enriched near the stop codon and 3' untranslated region (UTR) of coding genes in ES cells (Fig. 3h). Overall, these results indicate that an increased chromatin recruitment of *Mettl3* underlies the gains of m<sup>6</sup>A RNA methylation during paused pluripotency. However, we cannot exclude that *Mettl3* may also exert other functions at chromatin.

### **Mettl3 promotes mRNA decay during developmental pausing**

m<sup>6</sup>A methylation regulates numerous aspects of mRNA biology, including splicing, stability, translation and localization<sup>12,15,25,26</sup>. To dissect the function of m<sup>6</sup>A RNA methylation during pausing, we asked how changes in m<sup>6</sup>A affect mRNA levels during ES cell pausing. In the context of global hypotranscription in wild-type ES cells after pausing<sup>5</sup> (Fig. 2f), RNAs with increased m<sup>6</sup>A were significantly more downregulated than RNAs with decreased m<sup>6</sup>A (Fig. 4a). By contrast, this association was lost in *Mettl3*<sup>-/-</sup> cells when analysing the same genes (Fig. 4a). As m<sup>6</sup>A can control the expression of pluripotency genes in ES cells through RNA decay, we next examined whether such a mechanism also occurs during embryonic pausing. First, we re-analysed the RNA sequencing (RNA-seq) data from control and paused *Mettl3*<sup>+/+</sup> and *Mettl3*<sup>-/-</sup> ES cells to assess post-transcriptional regulation (Fig. 2f and Extended Data Fig. 2). Exonic reads reflect steady-state mature mRNAs, whereas intronic reads mostly represent pre-mRNAs. Comparing the difference between these has been shown to effectively quantify post-transcriptional regulation of gene expression<sup>27</sup> (Extended Data Fig. 5a–c). This analysis pointed to a global destabilization of the transcriptome when *Mettl3*<sup>+/+</sup> ES cells were induced to the paused state (Fig. 4b). By contrast, this global destabilization effect of pausing was lost in *Mettl3*<sup>-/-</sup> ES cells (Fig. 4b). To follow up on these insights, we performed a transcriptome-wide analysis of RNA decay kinetics by transiently labelling transcripts with a uridine analogue and tracking their dynamics over time (SLAM-seq method; Fig. 4c and Methods). In line with the exon and intron read analysis (Fig. 4a,b), paused *Mettl3*<sup>-/-</sup> ES cells displayed significantly longer RNA half-lives overall (Fig. 4c, Extended Data Fig. 5d and Supplementary Table 4). Importantly, an increase in RNA stability in paused *Mettl3*<sup>-/-</sup> ES cells was significantly associated with a gain in m<sup>6</sup>A and gene downregulation during pausing of wild-type ES cells (Fig. 4d,e and Extended Data Fig. 5e). We also validated for a subset of diagnostic mRNAs derived from the ES cell SLAM-seq data that this increase in stability also occurred in hormonally diapaused embryos (Fig. 4f). Taken together, these results indicate

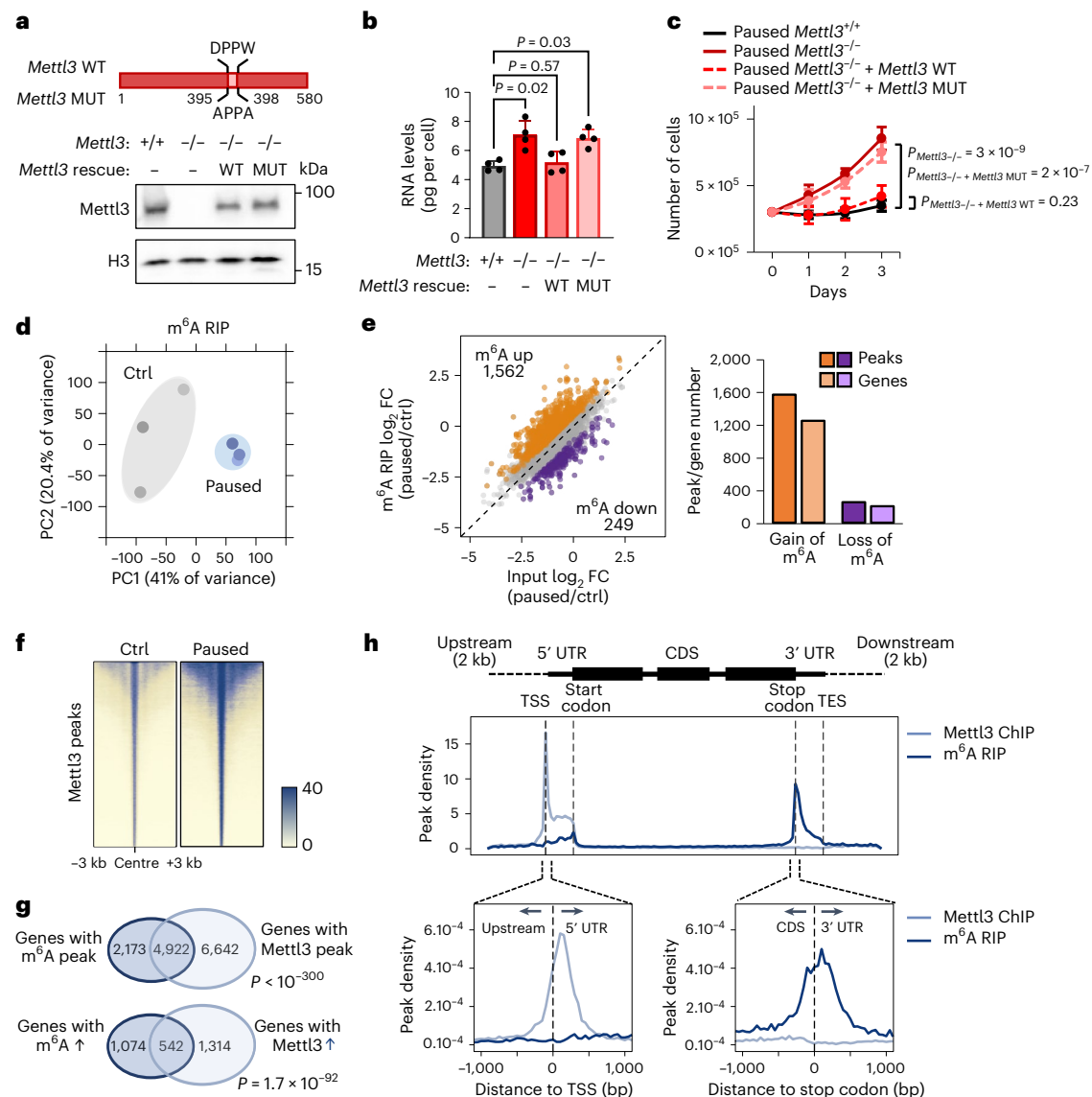


**Fig. 3 | The methyltransferase activity of Mettl3 sustains paused pluripotency.** **a**, Schematic of wild-type (WT) and catalytically inactive mutant (MUT) Mettl3 protein (top) and western blot of rescue by transfection in *Mettl3*<sup>-/-</sup> ES cells (bottom, representative of three biological replicates). **b, c**, Transfection with WT Mettl3, but not its catalytic mutant, restores the *in vitro* pausing phenotype of hypotranscription (**b**) and suppressed proliferation (**c**) in paused *Mettl3*<sup>-/-</sup> (p*Mettl3*<sup>-/-</sup>) ES cells ( $n = 4$  biological replicates). **d**, PCA plot for all m<sup>6</sup>A peaks across all samples by MeRIP-seq showing that paused ES cells have distinct m<sup>6</sup>A profiles ( $n = 3$  biological replicates per condition). **e**, MeRIP-seq shows increased m<sup>6</sup>A in paused ES cells. Scatter plot (left) and number of peaks/genes with significant gain and loss of m<sup>6</sup>A (right, fold change (FC) > 1.5 and adjusted  $P < 0.05$ ). **f**, Heatmaps of Mettl3 ChIP-seq signals in control and paused ES cells

showing increased Mettl3 binding in paused ES cells. Signals were merged from two biological replicates per condition. **g**, Venn diagrams showing significant overlap between target genes of m<sup>6</sup>A (on related RNA) and Mettl3 identifying all target genes (top) or genes with increased levels of m<sup>6</sup>A and Mettl3 (FC > 1.5, no statistical threshold) in paused ES cells (bottom). **h**, Metagenes profiles of peaks indicate that Mettl3 mainly targets the promoter and 5' UTR regions, whereas m<sup>6</sup>A mainly targets the stop codon and 3' UTR. CDS, coding sequence; TES, transcription end site. All data are mean  $\pm$  s.d. (**b, c**).  $P$  values (as indicated on figure) by one-way ANOVA with Dunnett's multiple comparison test (**b**), linear regression test with interaction (**c**), two-sided t-test adjusted by Benjamini-Hochberg FDR (**e**) or one-sided hypergeometric test (**g**).

that Mettl3-dependent m<sup>6</sup>A methylation is responsible for a global destabilization of the transcriptome in paused ES cells.

### N-Myc is a key 'anti-pausing' factor regulated by m<sup>6</sup>A

Our findings up to this point indicated that the transcriptionally dormant state of paused cells is imparted by a combination of reduced nascent transcription and increased transcript destabilization, effects that are muted in *Mettl3*<sup>-/-</sup> paused ES cells (Figs. 2 and 4 and Extended Data Fig. 6a,b). We proposed that m<sup>6</sup>A may contribute to the destabilization of mRNAs that encode putative 'anti-pausing' factors. To identify

such factors, we mined the RNA-seq, MeRIP-seq and SLAM-seq data for genes with the following characteristics: (1) gain m<sup>6</sup>A in paused ES cells; (2) are downregulated after pausing but to a lesser extent in *Mettl3*<sup>-/-</sup> ES cells; (3) are expressed at levels that are least two times higher in paused *Mettl3*<sup>-/-</sup> ES cells than in control paused ES cells; and (4) have an increased half-life in paused *Mettl3*<sup>-/-</sup> ES cells. This analysis identified 465 candidate anti-pausing factors (Extended Data Fig. 6c and Methods). We then took advantage of published data from early mouse embryos<sup>4</sup> to rank the candidates by their correlation with an expression signature of the m<sup>6</sup>A machinery. We reasoned that if these

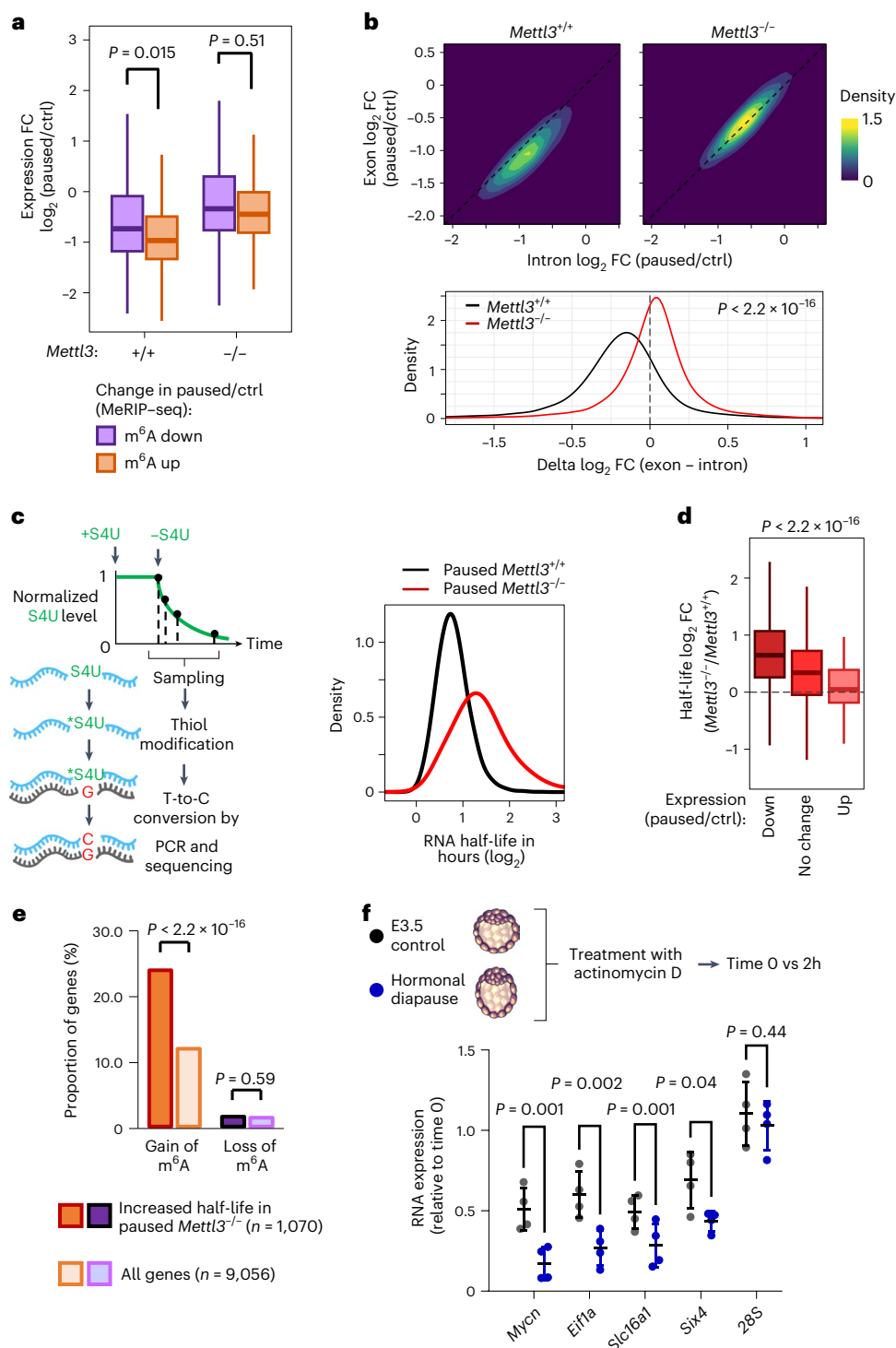


**Fig. 4 | Mettl3 promotes RNA destabilization during pausing.** **a**, RNAs with increased  $m^6A$  in pausing (as defined in Fig. 3e) are significantly more downregulated than RNAs with decreased  $m^6A$ . This pattern is Mettl3-dependent, as analysing the same RNAs in *Mettl3*<sup>-/-</sup> ES cells showed no effect. RNA-seq data as shown in Fig. 2f ( $n = 3$  biological replicates per group). **b**, Differences in expression ( $\log_2$  FC of paused/Ctrl) between exonic and intronic RNA-seq data indicate a global decrease in RNA stability in *Mettl3*<sup>-/-</sup> ES cells after pausing. This effect is absent in *Mettl3*<sup>+/+</sup> ES cells. **c**, Schematic of the measurement of RNA degradation kinetics by SLAM-seq (left). In the paused state, *Mettl3*<sup>-/-</sup> ES cells display an overall longer half-life of the transcriptome compared to *Mettl3*<sup>+/+</sup> ES cells (right). Half-lives were measured using four time points, with samples collected over two independent experiments (Extended Data Fig. 5d). S4U, 4-thiouridine. **d**, Changes in RNA expression during pausing

in WT ES cells (paused/ctrl, FC > 1.5) are anti-correlated with changes in RNA half-life in paused *Mettl3*<sup>-/-</sup> ES cells (as measured in Fig. 4c). **e**, RNAs with increased  $m^6A$  in pausing (as defined in Fig. 3e) are enriched among RNAs stabilized in *Mettl3*<sup>-/-</sup> ES cells (half-life FC > 1.5). **f**, Top, schematic of experiment. Bottom, Increased RNA stability in control E3.5 blastocysts compared to diapaused blastocysts, as measured by treatment with actinomycin D for 2 h followed by RT-qPCR ( $n = 4$  biological replicates). Ribosomal 28S was used as the negative control for RNA decay. All data are the mean  $\pm$  s.d.  $P$  values (as indicated on figure) by two-tailed Student's  $t$ -tests (**a, b, f**), one-way ANOVA (**d**) or two-proportion  $z$ -tests (**e**). Boxes in the box plots define the interquartile range (IQR) split by the median, with whiskers extending to the most extreme values within 1.5 $\times$  the IQR beyond the box.

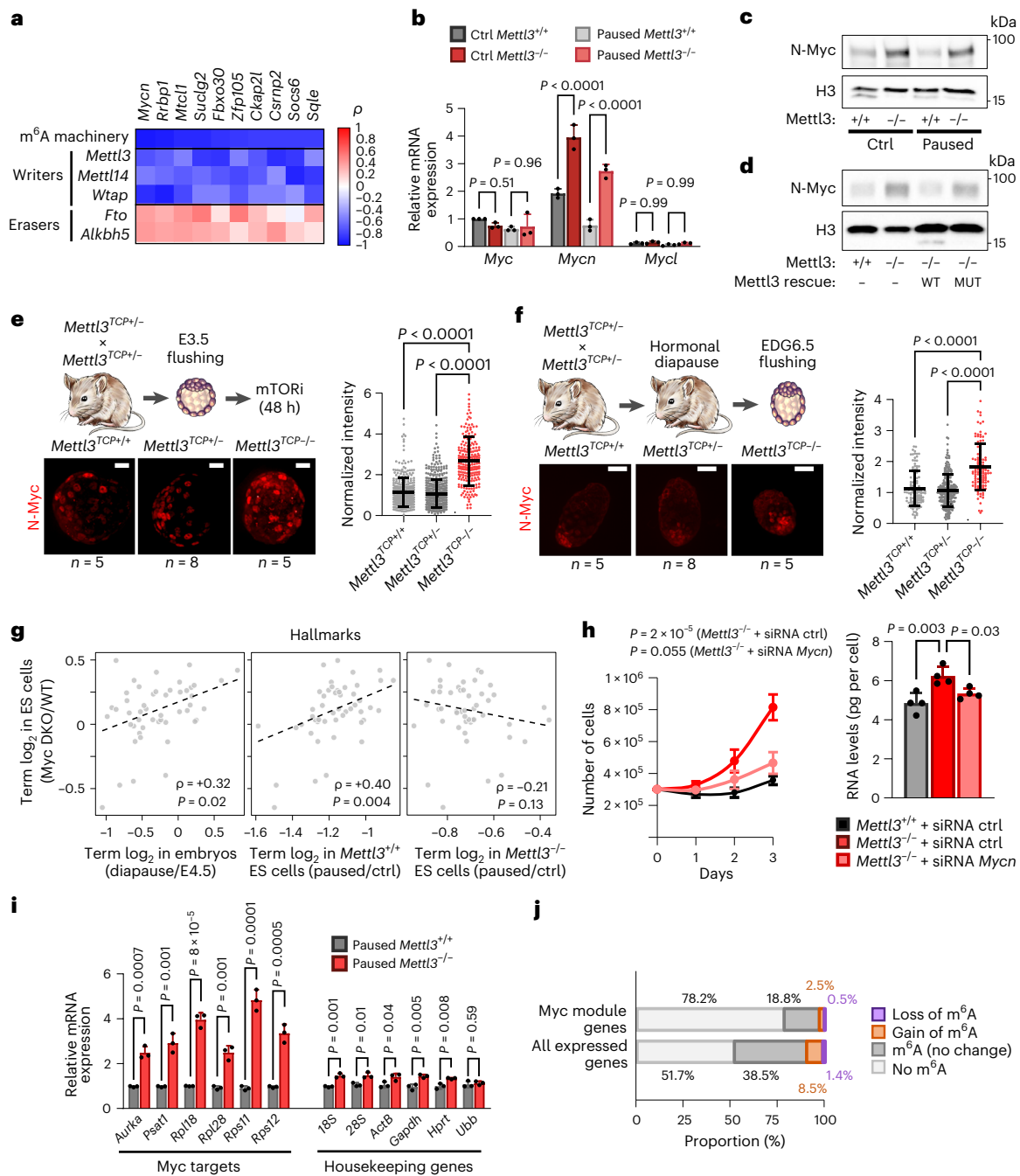


**Fig. 5 | The transcription factor N-Myc is a key mediator of the pausing defects of *Mettl3*<sup>-/-</sup> ES cells.** **a**, To identify m<sup>6</sup>A targets relevant in vivo, candidate genes were ranked by their Spearman’s correlation coefficient with the m<sup>6</sup>A machinery in early mouse embryos (Methods, *n* = 11 independent samples). The top ten ranked candidates are shown. **b,c**, Increased expression of N-Myc in *Mettl3*<sup>-/-</sup> ES cells, shown by RT-qPCR (**b**, *n* = 3 biological replicates) and western blot (**c**, representative of 4 biological replicates). **d**, Transfection with WT *Mettl3*, but not its catalytic mutant, restores N-Myc expression in *Mettl3*<sup>-/-</sup> ES cells (representative of three biological replicates). **e,f**, Top, schematics of experiments. Immunofluorescence images (left) and nuclear signal quantification (right) of N-Myc protein in ex vivo paused (**e**) and hormonally diapaused (**f**) blastocysts showing increased levels in *Mettl3*<sup>TCP-/-</sup>. Data are the mean ± s.d. Number of embryos (*n*) as indicated. Scale bar, 30 μm. **g**, Scatter plots of the median log<sub>2</sub> FC values for each ‘hallmark’ gene set showing a positive

correlation between *Myc/Mycn* DKO ES cells and diapaused embryos or paused *Mettl3*<sup>+/+</sup> (but not *Mettl3*<sup>-/-</sup>) ES cells, with Spearman’s correlation coefficient. **h**, Knockdown of *Mycn* restores the in vitro pausing phenotype of suppressed proliferation (left, *n* = 3 biological replicates) and total RNA levels per cell (right, *n* = 4 biological replicates) in paused *Mettl3*<sup>-/-</sup> ES cells. **i**, Nascent RNA capture by EU incorporation shows increased transcription for canonical *Myc* target genes in paused *Mettl3*<sup>-/-</sup> ES cells (*n* = 3 biological replicates). **j**, The majority of *Myc* module genes are not direct targets of m<sup>6</sup>A in paused pluripotency. The proportion in all expressed genes is shown for comparison. All data are the mean ± s.d. (**b,e,f,h,i**). *P* values (as indicated on figure) by two-way ANOVA with Tukey’s multiple comparisons test (**b**), one-way ANOVA with Dunnett’s multiple comparison tests (**e,f,h** right), two-sided Spearman’s correlation test (**g**), linear regression test with interaction (**h**, left) or two-way Student’s *t*-tests (**i**).

candidate genes are regulated by m<sup>6</sup>A in vivo, their expression should be anti-correlated with the expression of the methyltransferase complex and correlated with the expression of the m<sup>6</sup>A demethylation

machinery (Fig. 5a and Supplementary Table 5; see Methods for details). Notably, the top-ranked candidate from this analysis was *Mycn*, which codes for the N-Myc proto-oncogene (N-Myc) and was expressed at

high levels in both ES cells and embryos (Extended Data Fig. 6d,e). The Myc-regulated set of genes is a major module of the ES cell pluripotency network<sup>28</sup> and it is downregulated in diapause<sup>4,7</sup>. Importantly, Myc family members can act as global transcriptional amplifiers in the context of development and cancer<sup>28–30</sup>. We therefore investigated in-depth the regulation of *Mycn* by m<sup>6</sup>A RNA methylation and its potential impact in paused ES cells.

N-Myc expression was increased at the RNA and protein levels in paused *Mettl3*<sup>-/-</sup> ES cells (Fig. 5b,c and Extended Data Fig. 7a–c), and its expression was rescued by transfection of a catalytically active form of *Mettl3* (Fig. 5d and Extended Data Fig. 7d), which provided further support of its status as a m<sup>6</sup>A target. N-Myc levels were also increased in ex vivo paused and hormonally diapaused *Mettl3*<sup>-/-</sup> blastocysts compared with *Mettl3*<sup>+/-</sup> or *Mettl3*<sup>+/+</sup> embryos (Fig. 5e,f). Additionally, ES cells depleted for both c-Myc and N-Myc (Myc DKO) partially recapitulate gene expression changes in diapaused embryos and paused ES cells<sup>5,7</sup>, but this relationship was abolished in paused *Mettl3*<sup>-/-</sup> ES cells (Fig. 5g). In agreement with this result, the downregulation of Myc target genes that occurs after pausing was suppressed in *Mettl3*<sup>-/-</sup> ES cells (Fig. 2h). We therefore wondered whether increased Myc signalling contributes to the defective pausing observed in *Mettl3*<sup>-/-</sup> ES cells. Accordingly, knockdown of *Mycn* or treatment with the Myc inhibitor 10058-F4 both restored the decreases in proliferation and total RNA content in paused *Mettl3*<sup>-/-</sup> ES cells to levels equivalent to paused *Mettl3*<sup>+/-</sup> cells (Fig. 5h and Extended Data Fig. 7e–h). The downregulation of Myc target genes in pausing was imparted through reduced nascent transcription rather than by being directly targeted by m<sup>6</sup>A themselves (Fig. 5i,j), which is consistent with the established role of Myc as a transcriptional activator<sup>29,30</sup>. Taken together, these results indicate that N-Myc levels are downregulated in a m<sup>6</sup>A-dependent manner in paused ES cells. Moreover, the subsequent decrease in Myc signalling results in reduced transcriptional output and proliferation.

### m<sup>6</sup>A-methylated *Mycn* mRNA is targeted by the reader Ythdf2

To further probe the regulation of *Mycn* mRNA by methylation during pausing, we investigated the role of m<sup>6</sup>A readers. The m<sup>6</sup>A mark can affect mRNA metabolism through the binding of reader proteins, including the YTH domain family of proteins<sup>31–34</sup>. Knockout of the m<sup>6</sup>A reader Ythdf2 in particular closely phenocopied the defects in proliferation and RNA levels observed in paused *Mettl3*<sup>-/-</sup> ES cells (Extended Data Fig. 8a,b). As Ythdf2 can mediate the destabilization of m<sup>6</sup>A methylated mRNAs, including in ES cells<sup>12–14</sup>, we next examined whether Ythdf2 is responsible for the regulation of *Mycn* mRNA. We used our MeRIP-seq data (Fig. 6a) to further refine the site of m<sup>6</sup>A methylation and identified a hypermethylated m<sup>6</sup>A site near the stop codon of the *Mycn* mRNA (Extended Data Fig. 8c). RNA immunoprecipitation with quantitative

PCR (RIP-qPCR) revealed that *Mycn* mRNA is bound by both *Mettl3* and Ythdf2 in paused ES cells, and this binding was abolished by knockout of *Mettl3* (Extended Data Fig. 8d). Moreover, the half-life of *Mycn* mRNA was significantly increased in *Mettl3*<sup>-/-</sup> ES cells, specific to *Mycn* among the Myc family members, whereas no significant change in nascent transcription was observed (Fig. 6b and Extended Data Fig. 8e–g). A similar change in *Mycn* mRNA stability occurred in *Ythdf2*<sup>-/-</sup> ES cells (Extended Data Fig. 8h). Last, using a luciferase reporter assay, we found that the identified m<sup>6</sup>A site at the 3' end of *Mycn* mRNA conferred transcript destabilization in paused ES cells in a manner dependent on the integrity of the m<sup>6</sup>A site, as an A-to-C mutation nullified this effect (Fig. 6c). These results corroborate that m<sup>6</sup>A methylation regulates *Mycn* mRNA stability in paused ES cells through the binding of the Ythdf2 reader.

Finally, we explored how RNA methylation affects *Mycn* transcript stability and its downstream effects. We performed site-specific RNA demethylation using dCasRx-conjugated ALKBH5 (ref. 35) (Extended Data Fig. 9a–c). We validated that targeting dCasRx-ALKBH5 to the identified methylated site at the 3' end of *Mycn* mRNA results in decreased levels of m<sup>6</sup>A at this site in *Mettl3*<sup>+/-</sup> paused ES cells using two independent guide RNAs (gRNAs) (Extended Data Fig. 9d). Notably, global levels of m<sup>6</sup>A RNA were not affected by this approach (Extended Data Fig. 9e). Targeted demethylation of *Mycn* mRNA in *Mettl3*<sup>+/-</sup>-paused ES cells stabilized the transcript, which led to higher steady-state levels of N-Myc mRNA and protein (Fig. 6d,e and Extended Data Fig. 9f).

### *Mycn* mRNA demethylation recapitulates *Mettl3* loss

Notably, the targeted loss of m<sup>6</sup>A at *Mycn* mRNA was sufficient to increase levels of total RNA and proliferation in paused ES cells (Fig. 6f and Extended Data Fig. 9g). We further examined the transcriptional impact of *Mycn* mRNA stabilization by performing cell-number-normalized RNA-seq (Supplementary Table 6). We first confirmed that targeted demethylation of *Mycn* mRNA in paused ES cells leads to increased global transcriptional output (Fig. 6g and Extended Data Fig. 10a,b). Overall, transcriptional changes induced by *Mycn* mRNA stabilization significantly recapitulated those observed following the loss of *Mettl3*, particularly for upregulated genes (Fig. 6h,i). Notably, pathways enriched in paused ES cells with targeted demethylation of *Mycn* mRNA included both Myc targets and functional categories related to energy metabolism (Extended Data Fig. 10c), thereby further echoing the defects in hypotranscription observed in paused *Mettl3*<sup>-/-</sup> ES cells (Fig. 2h). Genes upregulated following *Mettl3* knockout and *Mycn* mRNA demethylation were both highly enriched for targets of N-Myc identified in wild-type ES cells by ChIP-seq<sup>36</sup> (Extended Data Fig. 10d,e). In conclusion, m<sup>6</sup>A demethylation of *Mycn* mRNA in

**Fig. 6 | *Mettl3* regulates pausing through m<sup>6</sup>A-mediated destabilization of *Mycn* mRNA. a**, Gene track view of MeRIP-seq and *Mettl3* ChIP-seq for *Mycn* mRNA. **b**, Increased *Mycn* mRNA stability in paused *Mettl3*<sup>-/-</sup> ES cells compared with paused *Mettl3*<sup>+/-</sup> ES cells as measured by an actinomycin D stability assay ( $n = 3$  biological replicates).  $t_{1/2}$ , half-life. **c**, Insertion of the identified *Mycn* m<sup>6</sup>A site, but not its mutated version, reduces transcript stability in paused ES cells as measured by a luciferase reporter assay ( $n = 5$  biological replicates). **d**, Site-specific demethylation of *Mycn*, achieved with a dCasRx conjugated to the m<sup>6</sup>A demethylase ALKBH5, directed by gRNAs (left), leads to increased *Mycn* mRNA stability (right,  $n = 3$  biological replicates). NT, non-targeting. **e,f**, Site-specific demethylation of *Mycn* phenocopies *Mettl3*<sup>-/-</sup> in paused ES cells, with increased expression of N-Myc by RT-qPCR (**e**, top,  $n = 7$  biological replicates) and western blot (**e**, bottom, representative of 3 biological replicates), and higher proliferation (**f**,  $n = 5$  biological replicates). **g**, Differential gene expression, as measured by RNA-seq, induced by targeted demethylation of *Mycn* mRNA in paused ES cells ( $n = 4$  biological replicates per condition, FC > 1.5 and adjusted  $P < 0.05$ ). **h**, Genes upregulated in paused *Mettl3*<sup>-/-</sup> ES cells (compared with paused *Mettl3*<sup>+/-</sup> ES cells) are also significantly upregulated following the

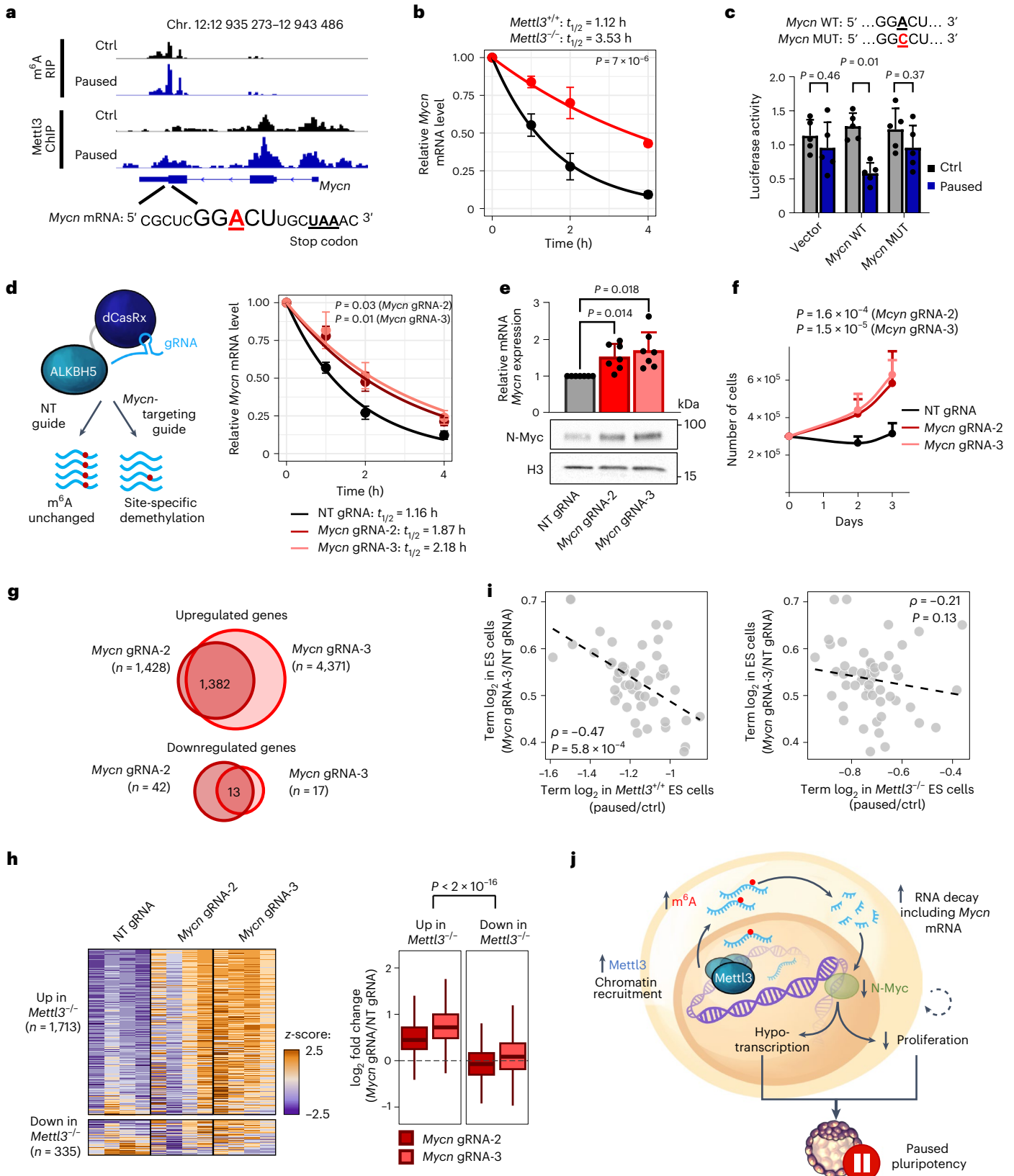
demethylation of *Mycn* mRNA. Number of genes ( $n$ ) as indicated. Data are z-score normalized per gene, with all samples displayed ( $n = 4$  biological replicates per group, left) and log<sub>2</sub> FC over NT gRNA control (right). **i**, Scatter plots of the median log<sub>2</sub> FC values for each 'hallmark' gene set, showing a significant negative correlation between paused ES cells with demethylated *Mycn* mRNA and paused *Mettl3*<sup>+/-</sup> (but not *Mettl3*<sup>-/-</sup>) ES cells. Spearman's correlation coefficient is indicated. **j**, Model of the role of *Mettl3*-dependent m<sup>6</sup>A methylation in paused pluripotency. Increased chromatin recruitment of *Mettl3* increases m<sup>6</sup>A in the transcriptome. Hypermethylation destabilizes many transcripts, including the mRNA encoding the anti-pausing factor N-Myc. In the absence of *Mettl3*, upregulated N-Myc enhances transcription and proliferation, disrupting pausing. All data are the mean ± s.d. (**c**, **e**, **f**) or mean ± s.e.m. (**b**, **d**).  $P$  values (as indicated on figure) by linear regression test with interaction (**b**, **d**, **f**), two-tailed paired Student's ratio  $t$ -tests (**c**), one-way ANOVA with Dunnett's multiple comparison tests (**e**), two-way ANOVA (**h**) or two-sided Spearman's correlation test (**i**). Box plots present centre lines as medians, with box limits as upper and lower quartiles and whiskers as 1.5× the IQR.

otherwise wild-type ES cells recapitulates the suppression of pausing observed in *Mettl3*<sup>-/-</sup> ES cells.

### Discussion

In summary, we showed here that *Mettl3*-dependent m<sup>6</sup>A RNA methylation is required for developmental pausing by maintaining

transcriptional dormancy (Fig. 6j). *Mettl3* does so through two interconnected mechanisms. First, *Mettl3*-dependent m<sup>6</sup>A RNA methylation promotes global mRNA destabilization, which leads to reduced levels of thousands of transcripts. Second, a direct target of m<sup>6</sup>A-mediated destabilization is the mRNA for the transcriptional amplifier N-Myc, which suppresses global nascent transcription. Our findings shed light



on the molecular mechanisms that underlie mammalian developmental pausing and reveal *Mettl3* as a key orchestrator of the crosstalk between transcriptomic and epitranscriptomic levels of gene regulation.

m<sup>6</sup>A RNA methylation has roles in other developmental contexts in which large-scale shifts in the transcriptional programme have to rapidly occur, notably in maternal-to-zygotic transition and exit from naive pluripotency<sup>12,37,38</sup>. The transition into diapause similarly involves substantial global downregulation and reprogramming of the transcriptome<sup>4,5</sup>. Moreover, a corresponding large-scale reversal of these transcriptional shifts is anticipated to occur following exit from diapause back into normal development<sup>39</sup>, although this transition is less well understood. We therefore posit that the biological function of m<sup>6</sup>A in developmental pausing may be twofold. First, m<sup>6</sup>A-mediated RNA decay may facilitate rapid changes in the mRNA levels of key master regulators of developmental timing, including *Mycn*, both in entry into and exit from diapause. Second, the integration of suppression of nascent transcription with transcript destabilization may constitute a more robust mechanism of hypotranscription than either process alone.

Notably, even though *Mettl3* methylates thousands of transcripts, we found that one target, *Mycn* mRNA, is key for its function in maintaining the suppressed transcriptional state of paused cells. Future studies may uncover additional functions of other m<sup>6</sup>A-regulated putative anti-pausing factors identified here.

In agreement with previous reports, our results support the notion that *Mettl3* acts at chromatin and methylates RNA co-transcriptionally<sup>23,24,40</sup>. Our data indicated that the global increase in m<sup>6</sup>A RNA levels after pausing is mediated by an increase in *Mettl3* recruitment to the chromatin, but it remains unclear how this process is regulated. Differential recruitment of *Mettl3* to chromatin may be mediated by interactions with transcription factors<sup>23,24</sup> and/or post-translational modifications<sup>41,42</sup>. It will be of interest to explore these or other possible mechanisms by which *Mettl3* and its partners may gain increased access to chromatin during diapause.

We anticipate that the regulatory relationship between m<sup>6</sup>A RNA methylation and cellular dormancy will have implications that extend beyond embryonic diapause. Modulations of mTOR signalling have been implicated in the control of stem cell dormancy in various embryonic and adult tissues<sup>43–45</sup>. Moreover, we and others have shown that cancer cells can enter a dormant state that is molecularly and functionally similar to diapause to survive chemotherapy<sup>46–48</sup>. The insights gained here, together with the recent development of small-molecule inhibitors targeting the m<sup>6</sup>A machinery<sup>49–51</sup>, provide exciting new opportunities to explore the biology of m<sup>6</sup>A RNA methylation in the fields of developmental biology, reproductive health, regenerative medicine and cancer.

## Online content

Any methods, additional references, Nature Portfolio reporting summaries, source data, extended data, supplementary information, acknowledgements, peer review information; details of author contributions and competing interests; and statements of data and code availability are available at <https://doi.org/10.1038/s41556-023-01212-x>.

## References

- Renfree, M. B. & Fenelon, J. C. The enigma of embryonic diapause. *Development* **144**, 3199–3210 (2017).
- van der Weijden, V. A. & Bulut-Karslioglu, A. Molecular regulation of paused pluripotency in early mammalian embryos and stem cells. *Front. Cell Dev. Biol.* **9**, 2039 (2021).
- Fenelon, J. C. & Renfree, M. B. The history of the discovery of embryonic diapause in mammals. *Biol. Reprod.* **99**, 242–251 (2018).
- Boroviak, T. et al. Lineage-specific profiling delineates the emergence and progression of naive pluripotency in mammalian embryogenesis. *Dev. Cell* **35**, 366–382 (2015).
- Bulut-Karslioglu, A. et al. Inhibition of mTOR induces a paused pluripotent state. *Nature* **540**, 119–123 (2016).
- Bulut-Karslioglu, A. et al. The transcriptionally permissive chromatin state of embryonic stem cells is acutely tuned to translational output. *Cell Stem Cell* **22**, 369–383 (2018).
- Scognamiglio, R. et al. Myc depletion induces a pluripotent dormant state mimicking diapause. *Cell* **164**, 668–680 (2016).
- Jiang, X. et al. The role of m<sup>6</sup>A modification in the biological functions and diseases. *Signal Transduct. Target Ther.* **6**, 74 (2021).
- Wang, P., Doxtader, K. A. & Nam, Y. Structural basis for cooperative function of *Mettl3* and *Mettl14* methyltransferases. *Mol. Cell* **63**, 306–317 (2016).
- Dominissini, D. et al. Topology of the human and mouse m<sup>6</sup>A RNA methylomes revealed by m<sup>6</sup>A-seq. *Nature* **485**, 201–206 (2012).
- Batista, P. J. et al. m<sup>6</sup>A RNA modification controls cell fate transition in mammalian embryonic stem cells. *Cell Stem Cell* **15**, 707–719 (2014).
- Geula, S. et al. m<sup>6</sup>A mRNA methylation facilitates resolution of naïve pluripotency toward differentiation. *Science* **347**, 1002–1006 (2015).
- Wang, Y. et al. N<sup>6</sup>-methyladenosine modification destabilizes developmental regulators in embryonic stem cells. *Nat. Cell Biol.* **16**, 191–198 (2014).
- Lasman, L. et al. Context-dependent compensation between functional Ythdf m<sup>6</sup>A reader proteins. *Genes Dev.* **34**, 1373–1391 (2020).
- Liu, J. et al. N<sup>6</sup>-methyladenosine of chromosome-associated regulatory RNA regulates chromatin state and transcription. *Science* **367**, 580–586 (2020).
- Chelmicki, T. et al. m<sup>6</sup>A RNA methylation regulates the fate of endogenous retroviruses. *Nature* **591**, 312–316 (2021).
- Wei, J. et al. FTO mediates LINE1 m<sup>6</sup>A demethylation and chromatin regulation in mESCs and mouse development. *Science* **376**, 968–973 (2022).
- Xu, W. et al. METTL3 regulates heterochromatin in mouse embryonic stem cells. *Nature* **591**, 317–321 (2021).
- Percharde, M., Bulut-Karslioglu, A. & Ramalho-Santos, M. Hypertranscription in development, stem cells, and regeneration. *Dev. Cell* **40**, 9–21 (2017).
- Hussein, A. M. et al. Metabolic control over mTOR-dependent diapause-like state. *Dev. Cell* **52**, 236–250 (2020).
- Sousa, M. I., Correia, B., Rodrigues, A. S. & Ramalho-Santos, J. Metabolic characterization of a paused-like pluripotent state. *Biochim. Biophys. Acta Gen. Subj.* **1864**, 129612 (2020).
- Sorci, M. et al. METTL3 regulates WTAP protein homeostasis. *Cell Death Dis.* **9**, 796 (2018).
- Barbieri, I. et al. Promoter-bound METTL3 maintains myeloid leukaemia by m<sup>6</sup>A-dependent translation control. *Nature* **552**, 126–131 (2017).
- Bertero, A. et al. The SMAD2/3 interactome reveals that TGFβ controls m<sup>6</sup>A mRNA methylation in pluripotency. *Nature* **555**, 256–259 (2018).
- Zhou, K. I. et al. Regulation of co-transcriptional pre-mRNA splicing by m<sup>6</sup>A through the low-complexity protein hnRNP G. *Mol. Cell* **76**, 70–81 (2019).
- Meyer, K. D. et al. 5' UTR m<sup>6</sup>A promotes cap-independent translation. *Cell* **163**, 999–1010 (2015).
- Gaidatzis, D., Burger, L., Florescu, M. & Stadler, M. B. Analysis of intronic and exonic reads in RNA-seq data characterizes transcriptional and post-transcriptional regulation. *Nat. Biotechnol.* **33**, 722–729 (2015).
- Kim, J., Chu, J., Shen, X., Wang, J. & Orkin, S. H. An extended transcriptional network for pluripotency of embryonic stem cells. *Cell* **132**, 1049–1061 (2008).

29. Kress, T. R., Sabò, A. & Amati, B. MYC: connecting selective transcriptional control to global RNA production. *Nat. Rev. Cancer* **15**, 593–607 (2015).
30. Percharde, M., Wong, P. & Ramalho-Santos, M. Global hypertranscription in the mouse embryonic germline. *Cell Rep.* **19**, 1987–1996 (2017).
31. Wang, X. et al. N<sup>6</sup>-methyladenosine-dependent regulation of messenger RNA stability. *Nature* **505**, 117–120 (2014).
32. Wang, X. et al. N<sup>6</sup>-methyladenosine modulates messenger RNA translation efficiency. *Cell* **161**, 1388–1399 (2015).
33. Xiao, W. et al. Nuclear m<sup>6</sup>A reader YTHDC1 regulates mRNA splicing. *Mol. Cell* **61**, 507–519 (2016).
34. Roundtree, I. A., Evans, M. E., Pan, T. & He, C. Dynamic RNA modifications in gene expression regulation. *Cell* **169**, 1187–1200 (2017).
35. Xia, Z. et al. Epitranscriptomic editing of the RNA N<sup>6</sup>-methyladenosine modification by dCasRx conjugated methyltransferase and demethylase. *Nucleic Acids Res.* **49**, 7361–7374 (2021).
36. Chen, X. et al. Integration of external signaling pathways with the core transcriptional network in embryonic stem cells. *Cell* **133**, 1106–1117 (2008).
37. Zhao, B. S. et al. m<sup>6</sup>A-dependent maternal mRNA clearance facilitates zebrafish maternal-to-zygotic transition. *Nature* **542**, 475–478 (2017).
38. Aguilo, F. et al. Coordination of m<sup>6</sup>A mRNA methylation and gene transcription by ZFP217 regulates pluripotency and reprogramming. *Cell Stem Cell* **17**, 689–704 (2015).
39. He, B. et al. Blastocyst activation engenders transcriptome reprogram affecting X-chromosome reactivation and inflammatory trigger of implantation. *Proc. Natl Acad. Sci. USA* **116**, 16621–16630 (2019).
40. Huang, H. et al. Histone H3 trimethylation at lysine 36 guides m<sup>6</sup>A RNA modification co-transcriptionally. *Nature* **567**, 414–419 (2019).
41. Sun, H. L. et al. Stabilization of ERK-phosphorylated METTL3 by USP5 increases m<sup>6</sup>A methylation. *Mol. Cell* **80**, 633–647 (2020).
42. Schöller, E. et al. Interactions, localization, and phosphorylation of the m<sup>6</sup>A generating METTL3–METTL14–WTAP complex. *RNA* **24**, 499–512 (2018).
43. Laplante, M. & Sabatini, D. M. mTOR signaling in growth control and disease. *Cell* **149**, 274–293 (2012).
44. Zhang, P. et al. mTOR is necessary for proper satellite cell activity and skeletal muscle regeneration. *Biochem. Biophys. Res. Commun.* **463**, 102–108 (2015).
45. Hu, J. K. H. et al. An FAK-YAP-mTOR signaling axis regulates stem cell-based tissue renewal in mice. *Cell Stem Cell* **21**, 91–106 (2017).
46. Rehman, S. K. et al. Colorectal cancer cells enter a diapause-like DTP state to survive chemotherapy. *Cell* **184**, 226–242 (2021).
47. Dhimolea, E. et al. An embryonic diapause-like adaptation with suppressed Myc activity enables tumor treatment persistence. *Cancer Cell* **39**, 240–256 (2021).
48. Liu, Y., Azizian, N. G., Sullivan, D. K. & Li, Y. mTOR inhibition attenuates chemosensitivity through the induction of chemotherapy resistant persisters. *Nat. Commun.* **13**, 7047 (2022).
49. Huang, Y. et al. Small-molecule targeting of oncogenic FTO demethylase in acute myeloid leukemia. *Cancer Cell* **35**, 677–691 (2019).
50. Yankova, E. et al. Small-molecule inhibition of METTL3 as a strategy against myeloid leukaemia. *Nature* **593**, 597–601 (2021).
51. Jeschke, J. et al. Downregulation of the FTO m<sup>6</sup>A RNA demethylase promotes EMT-mediated progression of epithelial tumors and sensitivity to Wnt inhibitors. *Nat. Cancer* **2**, 611–628 (2021).

**Publisher's note** Springer Nature remains neutral with regard to jurisdictional claims in published maps and institutional affiliations.

Springer Nature or its licensor (e.g. a society or other partner) holds exclusive rights to this article under a publishing agreement with the author(s) or other rightsholder(s); author self-archiving of the accepted manuscript version of this article is solely governed by the terms of such publishing agreement and applicable law.

© The Author(s), under exclusive licence to Springer Nature Limited 2023

## Methods

Procedures involving animals were performed according to the Animals for Research Act of Ontario and the Guidelines of the Canadian Council on Animal Care. Procedures conducted on animals were approved by The Animal Care Committee at The Centre for Phenogenomics, Toronto (TCP, protocol 22-0331).

### Mouse models

Mice were housed at 18–23 °C with 40–60% humidity, maintained on a 12-h light–dark cycle and with food and water ad libitum in individually ventilated units (Tecniplast) in the specific pathogen-free facility at the TCP.

The mouse line C57BL/6Ncr1-Mettl3<sup>em1(IMPC)Tcp/Tcp</sup> was generated as part of the Knockout Mouse Phenotyping Program (KOMP2) project at the TCP through the Cas9-mediated deletion of a 142 bp region (chromosome 14: 52299764–52299905 in ENSMUSE00001224053, GRCh38), which causes a frameshift and early truncation (I171Mfs\*4). The line was obtained from the Canadian Mouse Mutant Repository. Heterozygote mice (referred to as *Mettl3*<sup>TCP+/-</sup>) were maintained on a hybrid C57BL/6N×CD-1 background. Genotyping of mice was performed by Transnetyx.

For all embryo experiments, 6–12-week-old *Mettl3*<sup>TCP+/-</sup> female mice were mated with 6-week to 8-month-old *Mettl3*<sup>TCP+/-</sup> male mice. Collection and ex vivo culture of blastocysts was performed as previously described<sup>5</sup>, with pausing induced by flushing blastocysts at E3.5 with M2 and culturing them at 5% O<sub>2</sub>, 5% CO<sub>2</sub> at 37 °C in KSOM<sup>AA</sup>, with addition of 200 nM RapaLink-1 on the day after flushing. M2 (Millipore Sigma MR-015) and Life Global medium (Cooper Surgical LGGG-050) were provided by the TCP Transgenic Core. Blastocysts with a collapsed blastocoel were considered non-viable and collected for genotyping every day. Hormonal diapause was induced as previously described<sup>5</sup>, and blastocysts were collected at EDG6.5 or 8.5, imaged and genotyped. For genotyping of embryos, DNA was extracted from individual blastocysts using a Red Extract-N-Amp kit (Sigma) in a final volume of 36 µl. *Mettl3* status was assessed by PCR using 1 µl DNA extract in 15 µl total volume reaction with Phire Green Hot Start II PCR master mix (Thermo Fisher). The following cycling conditions were used: 98 °C for 30 s; 35 cycles of 98 °C for 5 s, 57 °C for 5 s and 72 °C for 5 s; and 72 °C for 1 min. See Supplementary Table 7 for primer sequences.

### Mouse ES cell culture

Mouse ES cells were grown on gelatin-coated plates in standard serum/LIF medium: DMEM GlutaMAX with sodium pyruvate, 15% FBS (Atlanta Biologicals), 0.1 mM non-essential amino acids, 50 U ml<sup>-1</sup> penicillin–streptomycin, 0.1 mM EmbryoMax 2-mercaptoethanol and 1,000 U ml<sup>-1</sup> ESGRO LIF (referred to as FBS/LIF medium). For FBS/LIF/2i culture, the FBS/LIF medium was supplemented with 1 µM PD0325901 and 3 µM CHIR99021. Pausing was induced by adding 200 nM INK128 to the medium as previously described<sup>5</sup>. Unless otherwise stated, ES cells were grown in FBS/LIF and paused for at least 5 days before use, and for exactly 2 weeks for all sequencing experiments.

### Cell models

E14 ES cells were provided by B. Skarnes (Sanger Institute) and derived as previously described<sup>52,53</sup>. HeLa (American Type Culture Collection (ATCC) CVCL\_0030) and HEK293T (ATCC CRL-3216) were provided by R. Blelloch and M. McManus (UCSF). *Mettl3* and *Ythdf1–Ythdf3* knockout ES cells were provided by J. Hanna<sup>12,14</sup>. Independent ES cell lines *Mettl3*<sup>-/-</sup> (numbers 2–4) cells were generated using the CRISPR–Cas9 method for validation of key results. Cloning was performed by annealing targeting oligonucleotides into pSpCas9(BB)-2A-GFP (PX458), a gift from F. Zhang (Addgene plasmid 48138; RRID:Addgene\_48138)<sup>54</sup>. E14 cells were transfected with Lipofectamine 2000, isolated by FACS, clonally expanded and validated for *Mettl3* loss.

Rescue experiments were performed by transfecting *Mettl3*<sup>-/-</sup> cells with pCDNA-FLAG-METTL3 or pCDNA-FLAG-METTL3-APPA using Lipofectamine 2000, followed by 3 days of selection with 250 µg ml<sup>-1</sup> geneticin. The plasmids were gifts from A. Fatica (Addgene plasmids 160250 and 160251; RRID:Addgene\_160250, RRID:Addgene\_160251)<sup>22</sup>.

ON-TARGETplus siRNAs against *Rptor*, *Rictor*, *Mycn* and non-targeting control (Horizon L-058754-01, L-064598-01, L-058793-01, D-001810-10, respectively) were transfected in a 6-well plate at a final concentration of 30 nM using Lipofectamine 2000 (Invitrogen).

### Site-specific m<sup>6</sup>A demethylation

HEK293T cells were transfected with pMSCV-dCasRx-ALKBH5-PURO and the viral packaging/envelope vectors pMD2.G and psPax2, gifts from Q. Xie and D. Trono (Addgene plasmids 175582, 12259 and 12260; RRID:Addgene\_175582; RRID:Addgene\_12259, RRID:Addgene\_12260)<sup>35</sup>. E14 cells were infected with pMSCV-dCasRx-ALKBH5-PURO lentivirus and selected with 2 µg ml<sup>-1</sup> puromycin. Clonal lines were selected for expression of dCasRx-ALKBH5 by western blotting. gRNAs were cloned using lenti-sgRNA-BSD, a gift from Q. Xie (Addgene plasmid 175583; RRID:Addgene\_175583)<sup>35</sup>. Each guide plasmid (1 µg) was transfected using Lipofectamine 2000 into dCasRx-ALKBH5-expressing cells in a 6-well plate. Cells were selected with 8 µg ml<sup>-1</sup> blasticidin for 3 days before use. See Supplementary Table 7 for primer sequences.

### Cell-number-normalized RNA analyses

Total RNA was extracted from an equal number of cells (typically  $\sim 2 \times 10^5$ ) using a RNeasy Micro kit with on-column DNase I digestion (Qiagen). Poly(A) RNA was extracted from  $1 \times 10^6$  cells using a Magnetic mRNA Isolation kit (NEB). The RNA concentration was measured using a Qubit RNA High Sensitivity kit. Complementary DNAs were generated using SuperScript IV VILO master mix using equal volumes of extracted RNAs, and qPCR data were acquired on a QuantStudio5 (Thermo Fisher Scientific). Unless otherwise stated, gene expression was cell-number normalized (CNN). See Supplementary Table 7 for primer sequences.

### CNN RNA-seq and data analysis

RNA extracted from an equal number of ES cells was spiked by adding 2 µl of 1:100 dilution of External RNAs Control Consortium (ERCC) Spike-in Mix1 (Thermo Fisher) to 10 µl of RNA (equivalent to  $\sim 1\text{--}2$  µg). Library preparation was done using a NEBNext Ultra II Directional Library Prep kit for Illumina with the mRNA Magnetic Isolation Module from 1 µg RNA, per the manufacturer's instructions (NEB). Sequencing was performed on a NextSeq500 (Illumina) with 75 bp single-end reads at the Lunenfeld–Tanenbaum Research Institute Sequencing Facility.

Libraries underwent adaptor trimming and quality check using Trim Galore! (v.0.4.0). Alignment to the mm10 transcriptome with ERCC sequences was performed using TopHat2 (v.2.0.13). Gene counts were obtained using the featureCounts function of subread (v.1.5.0) with options -t exon -g gene\_id. Raw counts were imported into R and normalized to ERCCs using edgeR (v.3.32.1)<sup>30,55</sup>. Data were further analysed using tidyverse (v.1.3.0) and plotted using ggplot2 (v.3.3.5). The significance threshold for differential expression was adjusted  $P < 0.05$  and absolute FC of  $> 1.5$ . Normalized counts were mean-centred per batch and log-transformed for PCA and heatmaps. GSEA was carried out with the fgsea package (v.1.16.0), with genes pre-ranked by  $t$ -values from the differential analysis (paused/ctrl). Gene set collections were downloaded from the Molecular Signatures Database (v.7.5.1; <http://www.gsea-msigdb.org/gsea/msigdb/index.jsp>). For intron analysis, RefSeq-annotated intronic regions were shortened by 50 bp on each side, and counts were obtained with featureCounts followed by analysis in R as for exons.

### Global m<sup>6</sup>A quantification

Nucleoside digestion was performed as previously described<sup>56</sup>. Separation was accomplished by reversed phase chromatography with an

Acquity UPLC HSS T3 (Waters) on a Vanquish Flex Quaternary UHPLC system (Thermo Fisher Scientific). Mass spectrometry was performed on a Quantiva triple quadrupole mass spectrometer interfaced with a H-ESI electrospray source (Thermo Fisher Scientific). Data were analysed with Tracefinder 4.1 (Thermo Fisher Scientific) and Qual browser of Xcalibur 3.0. The mass transitions (precursor  $\rightarrow$  product) for  $m^6A$  were 282  $\rightarrow$  94, 282  $\rightarrow$  123 and 282  $\rightarrow$  150.

Changes in  $m^6A$  levels were also measured by dot blot from 50 ng of poly(A) RNA. Blotting was performed as previously described<sup>57,58</sup>, except that Diagenode C15410208 (1:400) was used as the primary antibody.

### $m^6A$ MeRIP-seq

MeRIP was done using an EpiMark  $N^6$ -methyladenosine Enrichment kit with 4  $\mu$ g spiked poly(A) RNA of ES cells spiked with 2% of human cells (HeLa). Specificity of the immunoprecipitate was verified using  $m^6A$ -modified and unmodified exogenous controls per the manufacturer's instructions. The normalization approach with human cells was validated beforehand by spiking ES cells with 1, 2 or 4% human cells (Extended Data Fig. 3b).  $m^6A$  enrichment was measured by qPCR with reverse transcription (RT-qPCR) in three mouse mRNAs (*Neurod1*, *Nr5a2* and *Sox1*) known to be methylated in ES cells<sup>32</sup> and normalized to the average levels of five highly expressed and methylated human mRNAs (*HSBP1*, *PCNX3*, *GBA2*, *ITMB2* and *PCBP1*)<sup>51</sup>. MeRIP libraries were constructed from 0.5–1 ng of input or immunoprecipitated RNA and prepared using a SMART-seq RNA library prep v.2 kit (TakaraBio) per the manufacturer's recommendations. Samples were sequenced on a HiSeq 4000 using single-end 50 bp reads at the UCSF Center for Advanced Technology.

Pre-processing of sequencing data was performed similarly to the RNA-seq data, but with reads unmapped to mm10 being aligned to hg19. For input samples, gene expression was normalized as for CNN RNA-seq, except that the ratio of hg19/mm10 reads was used for normalization instead of ERCCs. For  $m^6A$  RIP samples, peaks were called with MACS2 (with immunoprecipitated samples and their input counterpart as controls and  $q < 0.01$ ). Peaks were annotated by intersecting centre positions with RefSeq annotations. Peak analysis was performed using DiffBind (v.3.0.15), with the options `minOverlap=2`, `Score=DBA_SCORE_READS`. MeRIP peaks were then first normalized using the ratio of hg19/mm10 reads in each sample for normalization, then adjusted by dividing values by the ratio  $\text{Input}_{\text{sample}}/\text{Input}_{\text{average}}$  of the corresponding gene to consider expression changes. In the following differential analysis with edgeR, these normalized  $m^6A$  levels were protected from further re-scaling by fixing the library size for all samples as `lib.size = rep(10^6, 6)` in the voom function. The threshold for significant differential expression was adjusted  $P < 0.05$  and absolute FC of  $>1.5$ . For motif analysis, peaks were limited to 100 bp surrounding the centre and submitted to DREME of the Meme-suite (<http://meme-suite.org>). Bigwig files were generated using DeepTools (v.3.3.0) and visualized in Integrated Genome Viewer (IGV v.2.9.4), with the vertical scale adjusted to consider expression changes individually for each gene.

### Site-specific quantification of $m^6A$

We identified a putative  $m^6A$  site within the *Mycn* MeRIP peak using the  $m^6A$ -Atlas database (<http://www.xjtlu.edu.cn/biologicalsciences/atlas>)<sup>59</sup>. We measured  $m^6A$  levels by RT-qPCR, exploiting the diminished capacity of Bst to retrotranscribe  $m^6A$  residues compared with the MRT control enzyme, and RT primers targeting immediately before or after the site (+ or -, respectively)<sup>60,61</sup>. cDNA was generated with -100 ng of total RNA, 100 nM primer (+ or -), 50  $\mu$ M dNTPs and 0.1 U of Bst3.0 (NEB) or 0.8 U of MRT (Thermo Scientific). The cycling conditions were 50 °C for 15 min, 85 °C for 3 min, then 4 °C. RT-qPCR data were normalized as  $(2^{-(C_{\text{Bst}}^- - C_{\text{MRT}}^-)} - 2^{-(C_{\text{Bst}}^+ - C_{\text{MRT}}^+)}) / 2^{-(C_{\text{Bst}}^- - C_{\text{MRT}}^-)}$ . Negative values were considered below the detection threshold and rounded to 0.

### Mettl3 ChIP-seq

ES cells were spiked with 2% of human cells (HeLa), then crosslinked in 1% formaldehyde-PBS for 10 min at room temperature. After quenching with 125 mM glycine for 5 min at room temperature, followed by 15 min at 4 °C, cells were washed in cold PBS and stored at -80 °C. Cells were diluted at 5 million cells per 100  $\mu$ l in shearing buffer (1% SDS, 10 mM EDTA, 50 mM Tris-HCl pH 8.0, 5 mM NaF, Halt Protease Inhibitor Cocktail (Thermo Fisher) and 1 mM PMSF), rotating at 4 °C for 30 min, then 100  $\mu$ l of lysate was passed into a microTUBE AFA Fiber Snap-Cap (Covaris). Chromatin was sheared to 200–500 bp fragments on a Covaris E220 with settings PIP 175, duty 10%, CPB 200, for 7 min. Immunoprecipitation was performed overnight using 200  $\mu$ l of each lysate (approximate chromatin from 10 million cells) and 5  $\mu$ g of antibody (Proteintech 15073-1-AP), following the iDeal ChIP-seq kit for Transcription Factors (Diagenode) protocol. Elution, de-crosslinking and DNA purification were performed per instructions. Libraries were constructed from -2 ng DNA using a NEBNext Ultra II DNA Library Prep kit for Illumina (NEB). Samples were sequenced on a NextSeq500 (Illumina) with 75 bp single-end reads at the Lunenfeld-Tanenbaum Research Institute Sequencing Facility.

Reads were trimmed of adaptors using Trim Galore! (v.0.4.0) and aligned to mm10 using bowtie2 (v.2.2.5131). Unmapped reads were then mapped to hg19. SAM files were converted to BAM files, sorted and indexed using samtools (v.1.9). BAM files were deduplicated using MarkDuplicates (picard (v.2.18.14)). Peaks were called with MACS2 (using immunoprecipitated samples and their input as controls) with the options `--gsize 3.0e9 -q 0.05 --nomodel --broad` and annotated by intersecting centre positions with RefSeq annotations. The most upstream and downstream annotated TSS and TES, respectively, were considered for each gene. Peak analysis was performed using DiffBind (v.3.0.15) with `Score=DBA_SCORE_TMM_READS_FULL_CPM`. Normalization was done using edgeR with the ratio of mm10/hg19 reads (relative to the respective input sample). For TSS analysis, a 1 kb window surrounding the TSS of every RefSeq gene was used. Bigwig files were generated using DeepTools (v.3.3.0) with `--scaleFactor` for normalization and visualized in IGV (v.2.9.4).

### SLAM-seq

RNA decay was measured using the SLAM-seq Kinetics Kit-Catabolic Kinetics Module (Lexogen)<sup>62</sup>. In brief,  $8 \times 10^5$  paused mouse ES cells were seeded in a 6-well plate. After 12 h, the cells were incubated in standard paused medium supplemented with 100  $\mu$ M S4U, protected from light and with medium exchange every 3 h. After 12 h of labelling, the medium was changed back to standard paused medium without S4U and cells were collected at the indicated time points, followed by total RNA isolation using phenol-chloroform extraction. RNA samples were treated with 10 mM iodoacetamide, ethanol precipitated and subjected to Quant-seq 3'-end mRNA library preparation (Lexogen) using 100 ng RNA.

Reads were trimmed and mapped to the mouse genome (GRCm38/mm10) using the Next Flow (v.22.10.6) SLAM-seq pipeline (v.1.0.0) with `-profile singularity`, `-read_length 100`, and a 3' UTR exons table was downloaded from the UCSC genome browser<sup>63-65</sup>. 3' UTR counts were then analysed using edgeR, as detailed for RNA-seq, with T-to-C conversion counts being normalized to total counts. Expression values were then fitted to an exponential decay model using linear regression in R.

### Screening for $m^6A$ targets

The following selection criteria were applied: (1) gain of  $m^6A$  in pausing (MeRIP-seq:  $\log_2(\text{FC}) > 0$ ); (2) downregulation suppressed in *Mettl3*<sup>-/-</sup> ES cells (RNA-seq:  $\log_2(\text{FC}_{\text{Mettl3}^{+/+}}) < 0$  and  $\log_2(\text{FC}_{\text{Mettl3}^{+/+}}) < \log_2(\text{FC}_{\text{Mettl3}^{-/-}})$ ); (3) expression at least 2 times higher in paused *Mettl3*<sup>-/-</sup> ES cells (RNA-seq:  $\text{CP}_{\text{Mettl3}^{-/-}} > 2 \times \text{CP}_{\text{Mettl3}^{+/+}}$ ); (4) RNA more stable in paused *Mettl3*<sup>-/-</sup> ES cells (SLAM-seq:  $\log_2(\text{FC}_{\text{exon}}) > 1.5 \times \log_2(\text{FC}_{\text{intron}})$ ). Then, using published RNA-seq data from mouse embryos<sup>4</sup>, we averaged the

z-scores of the writers (*Mettl3*, *Mettl14* and *Wtap*) and the z-scores of the erasers (*Fto* and *Alkbh5*) multiplied by  $-1$ . Finally, we ranked all targets by their Spearman's correlation coefficients with this  $m^6A$  machinery signature, focusing on genes with negative correlations.

### RIP analysis

In total, 2  $\mu\text{g}$  anti-Mettl3, Ythdf2 or control IgG antibodies were pre-bound to 20  $\mu\text{l}$  Protein A Dynabeads (Thermo Fisher), rotating for 3 h at 4 °C. Beads were collected on a DynaMag (Thermo Fisher) and resuspended in RIP buffer (150 mM KCl, 25 mM Tris pH 7.4, 5 mM EDTA, 0.5 mM DTT, 0.5% NP40, protease and RNase inhibitors) containing 500  $\text{ng ml}^{-1}$  rRNA (Thermo Fisher) and 1  $\text{mg ml}^{-1}$  BSA to block for 30 min. ES cells were collected and lysed in RIP buffer on ice for 20 min. Supernatants (500  $\mu\text{l}$ , equivalent to 10 million cells) were pre-cleared with 20  $\mu\text{l}$  Protein A Dynabeads, rotating for 30 min at 4 °C. Cleared lysates were incubated together with antibody-bound blocked beads overnight at 4 °C. Lysates were washed 5 times in RIP buffer, and RNA was extracted using Direct-zol RNA kits (Zymo Research) before analysing by RT-qPCR.

### Western blot analysis

Whole-cell and chromatin extract were prepared as previously described<sup>66,67</sup>. Denatured samples were separated on 4–15% Mini-Protean TGX SDS-PAGE gels and transferred to nitrocellulose membranes using wet transfer. Membranes were blocked in 5% milk-TBS-T and incubated with primary antibodies overnight at 4 °C. HRP-conjugated secondary antibodies were incubated for 1 h at room temperature. Protein detection was performed using ECL (Pierce) or Clarity Max (Bio-Rad). Quantification of bands was done using ImageJ. See Supplementary Table 6 for antibody details.

### mRNA stability assay

Cells were treated with 5  $\mu\text{g ml}^{-1}$  actinomycin D for 0, 1, 2 or 4 h. RNA level was measured by RT-qPCR and normalized to *Actb*. Expression values were fitted to an exponential decay model using linear regression in R.

For embryo experiments, 8–10 blastocysts were collected immediately or cultured for 2 h in KSOM with 5  $\mu\text{g ml}^{-1}$  actinomycin D. RNA was extracted using a PicoPure RNA Extraction kit. Embryo RT-qPCR data were normalized to time 0 using *Actb* as a reference gene.

### Luciferase reporters of RNA stability

The region surrounding the identified  $m^6A$  site of *Mycn* mRNA (wild-type sequence or A-to-C mutation) was cloned into the pmirGLO Dual-Luciferase miRNA target expression vector (Promega). Vector (500 ng) was transfected in ES cells in a 6-well plate with Lipofectamine 2000 and cells were lysed after 48 h. Firefly luciferase signals were measured with a luminometer and normalized to Renilla luciferase activity with a Dual-Glo Luciferase Assay system.

### Nascent transcription assays in ES cells

To assess global transcriptional output, cells were treated with 1 mM EU for 45 min, collected by trypsinization and prepared following the Click-iT RNA Alexa Fluor 488 Imaging kit (Thermo Fisher) instructions. Data were collected by flow cytometry using a Beckman Coulter Gallios and analysed using Kaluza. Fluorescence values were plotted as the median MFI per sample relative to control *Mettl3*<sup>+/+</sup> cells.

For nascent RNA capture, EU incubation was performed in ES cells as described above. Cells were collected by trypsinization, counted and  $2 \times 10^5$  cells were used to extract RNA. Biotinylated nascent RNA was captured according to protocols within the Click-iT Nascent RNA Capture kit (Invitrogen) and used for RT-qPCR.

### Embryo immunofluorescence

Ex vivo paused embryos were labelled with 1 mM EU for 45 min for nascent transcription and fixed in 4% paraformaldehyde for 15 min.

Permeabilization was done with 0.5% Triton X-100 in PBS–5% FBS for 15 min. After blocking in PBS–2.5% BSA with 5% donkey serum for 1 h, embryos were incubated overnight at 4 °C with primary antibodies (Mettl3, Abcam ab195352 1/200; N-Myc, Cell Signaling Technology D1V2A 1/200). EU fluorescence coupling was performed per the manufacturer's instructions for the Click-iT RNA Alexa Fluor 488 Imaging kit. Embryos were incubated with fluorescence-conjugated secondary antibodies for 1 h at room temperature, stained with 4,6-diamidino-2-phenylindole (DAPI) in fresh blocking, washed and transferred to M2 medium ( $\sim 5 \mu\text{l}$ ). Images were captured using a Leica DMI 6000 spinning disk confocal microscope, and embryos were genotyped. Quantification was performed in ImageJ, with 10 image planes stacked by 'average intensity' projection, repeated 4 times (40 planes used per embryo in total). Nuclei were quantified using the ROI Manager, and background values were subtracted. Values were normalized to the average of *Mettl3*<sup>TC<sup>+/+</sup></sup> embryos within each litter to avoid batch effects.

### Statistics and reproducibility

Statistical analyses were performed in GraphPad Prism (v.9.3.1) or R (v.4.0.3). Data are presented as the mean  $\pm$  s.d. or s.e.m., except where otherwise indicated. Data distribution was assumed to be normal, but this was not formally tested. Box plots present centre lines as medians, with box limits as upper and lower quartiles and whiskers as  $1.5 \times$  the IQR. Two-tailed Student's *t*-test and one-way or two-way ANOVA with Dunnett's multiple comparison tests were used when normal distribution could be assumed. Time series were modelled by linear regression on  $\log_2$ -transformed *y* values, with *P* values extracted from the interaction between time and the categorical variable of interest. GSEA was performed with fGSEA in R, with the adjusted *P* values as indicated. Correlation was measured by  $\rho$  Spearman's rank correlation coefficient.

All replicates for in vitro data are derived from independent experiments, with a subpopulation of parental cells allocated randomly to control or treatment without specific randomization methods. All replicates for in vivo data are derived from at least three embryos per genotype and two separate litters. No randomization was required for design of in vivo experiments, as embryos were collected, cultured and treated together and only later identified by *Mettl3* genotype. No statistical methods were used to predetermine sample sizes, but our sample sizes were similar to those reported in previous publications<sup>5,55,58</sup>. Data collection and analyses were not performed blind to the conditions of the experiments. Two samples were excluded from the SLAM-seq analysis owing to abnormally low sequencing depth.

### Reporting summary

Further information on research design is available in the Nature Portfolio Reporting Summary linked to this article.

### Data availability

Sequencing data have been deposited into the NCBI Gene Expression Omnibus (GEO) repository (<http://ncbi.nlm.nih.gov/geo>) under accession number GSE202848. Mass spectrometry data have been deposited into the Metabolights database (<https://www.ebi.ac.uk/metabolights>) under the identifier MTBLS8041. Published RNA-seq and ChIP-seq data used in this study are available under the accession numbers E-MTAB-2958 (early mouse embryos), E-MTAB-3386 (*Myc/Mycn* DKO ES cells) and GSE11431 (N-Myc ChIP). Examples of FACS gating have been deposited into the Figshare repository (<https://doi.org/10.6084/m9.figshare.23551986>). Mouse and human reference genomes (mm10 and hg19, respectively) were downloaded from the UCSC browser (<https://genome.ucsc.edu/>). All other data supporting the findings of this study are available from the corresponding authors on reasonable request. Source data are provided with this paper.

## Code availability

Code supporting this study are available at a dedicated GitHub repository ([https://github.com/EvelyneCollignon/Mettl3\\_pausing](https://github.com/EvelyneCollignon/Mettl3_pausing)) and at Zenodo (<https://doi.org/10.5281/zenodo.8068381>).

## References

52. Nichols, J., Evans, E. P. & Smith, A. G. Establishment of germ-line-competent embryonic stem (ES) cells using differentiation inhibiting activity. *Development* **110**, 1341–1348 (1990).
53. Handyside, A. H., O'Neill, G. T., Jones, M. & Hooper, M. L. Use of BRL-conditioned medium in combination with feeder layers to isolate a diploid embryonic stem cell line. *Roux Arch. Dev. Biol.* **198**, 48–56 (1989).
54. Ran, F. A. et al. Genome engineering using the CRISPR–Cas9 system. *Nat. Protoc.* **8**, 2281–2308 (2013).
55. Macrae, T. A. & Ramalho-Santos, M. The deubiquitinase Usp9x regulates PRC2-mediated chromatin reprogramming during mouse development. *Nat. Commun.* **12**, 1865 (2021).
56. Ross, R., Cao, X., Yu, N. & Limbach, P. A. Sequence mapping of transfer RNA chemical modifications by liquid chromatography tandem mass spectrometry. *Methods* **107**, 73–78 (2016).
57. Delatte, B. et al. Transcriptome-wide distribution and function of RNA hydroxymethylcytosine. *Science* **351**, 282–285 (2016).
58. DiTroia, S. P. et al. Maternal vitamin C regulates reprogramming of DNA methylation and germline development. *Nature* **573**, 271–275 (2019).
59. Tang, Y. et al. m<sup>6</sup>A-Atlas: a comprehensive knowledgebase for unraveling the N<sup>6</sup>-methyladenosine (m<sup>6</sup>A) epitranscriptome. *Nucleic Acids Res.* **49**, D134–D143 (2021).
60. Castellanos-Rubio, A. et al. A novel RT-QPCR-based assay for the relative quantification of residue specific m<sup>6</sup>A RNA methylation. *Sci. Rep.* **9**, 4220 (2019).
61. Olazagoitia-Garmendia, A. & Castellanos-Rubio, A. Relative quantification of residue-specific m<sup>6</sup>A RNA methylation using m<sup>6</sup>A-RT-QPCR. *Methods Mol. Biol.* **2298**, 185–195 (2021).
62. Neumann, T. et al. Quantification of experimentally induced nucleotide conversions in high-throughput sequencing datasets. *BMC Bioinformatics* **20**, 258 (2019).
63. DI Tommaso, P. et al. Nextflow enables reproducible computational workflows. *Nat. Biotechnol.* **35**, 316–319 (2017).
64. Ewels, P. A. et al. The nf-core framework for community-curated bioinformatics pipelines. *Nat. Biotechnol.* **38**, 276–278 (2020).
65. Kurtzer, G. M., Sochat, V. & Bauer, M. W. Singularity: scientific containers for mobility of compute. *PLoS ONE* **12**, e0177459 (2017).
66. Sadowski, H. B. & Gilman, M. Z. Cell-free activation of a DNA-binding protein by epidermal growth factor. *Nature* **362**, 79–83 (1993).
67. Méndez, J. et al. Human origin recognition complex large subunit is degraded by ubiquitin-mediated proteolysis after initiation of DNA replication. *Mol. Cell* **9**, 481–491 (2002).

## Acknowledgements

We thank members of the Santos Laboratory, D. Schramek, A. Bulut-Karslioglu, T. Macrae, J. Jeschke and F. Fuks for feedback on the manuscript; members of the Hanna Laboratory for providing cells; members of the UCSF Center for Advanced Technology and the LTRI Sequencing Core for next-generation sequencing; staff at the LTRI Flow Cytometry Facilities, A. Bulut-Karslioglu and S. Biechele for advice on diapause; M. Percharde and T. Macrae for bioinformatics guidance; and staff at the TCP Transgenic Core for providing timed pregnant animals and the TCP Animal Resources for colony management. E.C. was supported by a fellowship from the Belgian American Educational Foundation. P.A.L. is funded by the US National Institutes of Health (NIH, GM58843). This work was supported by grant R01GM113014 from the NIH, a Canada 150 Research Chair in Developmental Epigenetics, the Great Gulf Homes Charitable Foundation, and project grants 165935 and 178094 from the Canadian Institutes of Health Research (to M.R.-S.).

## Author contributions

E.C. and M.R.-S. conceived the project and designed experiments. E.C. performed the majority of the experiments and interpreted data. B.C. performed EU flow cytometry and embryo imaging. G.F. generated knockout ES cells and induced mouse hormonal diapause. J.F.-R. performed lentiviral infection and chromatin shearing. E.C., S.-B.M. and S.A.M. performed SLAM-seq. P.A.L. and R.L.R. performed mass spectrometry. M.R.-S. supervised the project. E.C. and M.R.-S. wrote the manuscript with feedback from all authors.

## Competing interests

The authors declare no competing interests.

## Additional information

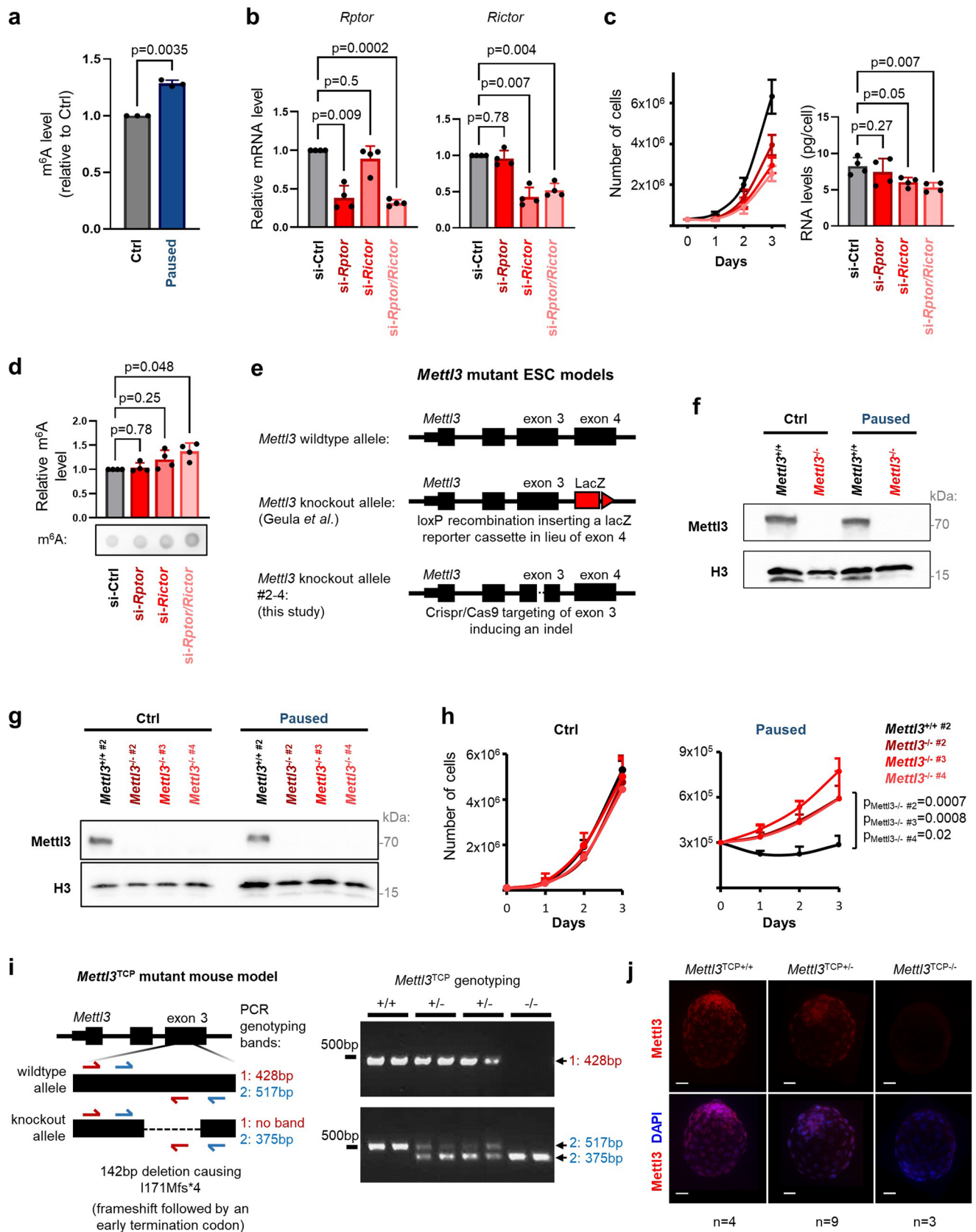
**Extended data** is available for this paper at <https://doi.org/10.1038/s41556-023-01212-x>.

**Supplementary information** The online version contains supplementary material available at <https://doi.org/10.1038/s41556-023-01212-x>.

**Correspondence and requests for materials** should be addressed to Evelyne Collignon or Miguel Ramalho-Santos.

**Peer review information** *Nature Cell Biology* thanks Jacob Hanna, Baoming Qin, and the other, anonymous, reviewer(s) for their contribution to the peer review of this work. Peer reviewer reports are available.

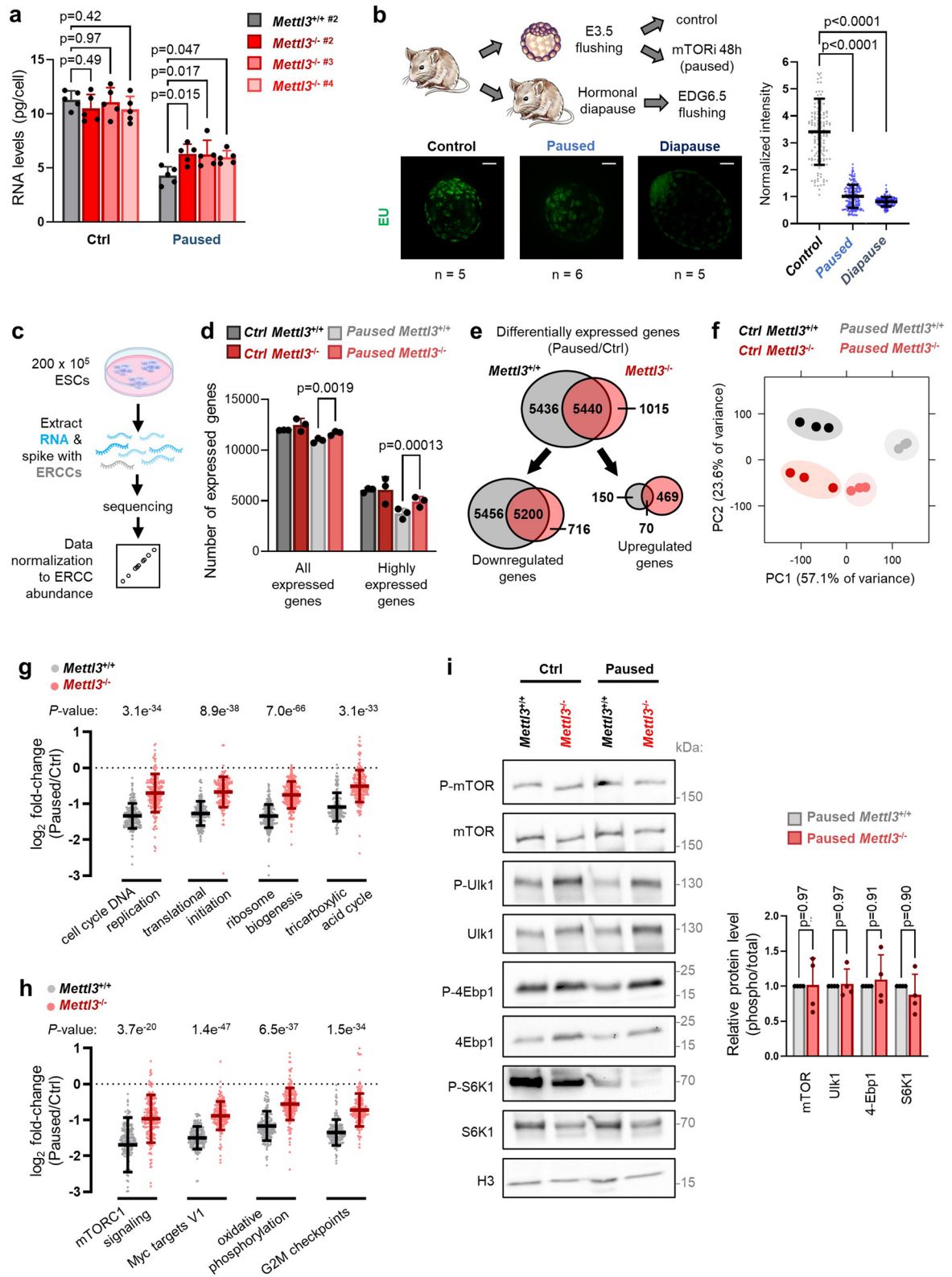
**Reprints and permissions information** is available at [www.nature.com/reprints](http://www.nature.com/reprints).



Extended Data Fig. 1 | See next page for caption.

**Extended Data Fig. 1 | Dissection of paused pluripotency in *Mettl3*<sup>-/-</sup> models.** **a.** m<sup>6</sup>A increase in paused ESCs was validated in an independent mass spectrometry experiment. Levels relative to control (Ctrl) for each replicate are shown (n = 3 biological replicates). **b.** Validation of *Rptor* and *Rictor* knockdown by RT-qPCR in paused ESCs grown in FBS/LIF/2i (n = 4 biological replicates). **c.** mTOR inhibition by *Rptor* and *Rictor* knockdown induces a paused phenotype with reduced cell proliferation and total RNA levels (n = 4 biological replicates). **d.** Dot blot showing an increase in m<sup>6</sup>A levels in ESCs upon knockdown of *Rptor* and *Rictor*. Levels of m<sup>6</sup>A are normalized to RNA loading control (methylene blue staining, n = 4 biological replicates). **e.** Design of *Mettl3*<sup>-/-</sup> ESCs models used in this study. **f.** Validation of *Mettl3*<sup>-/-</sup> ESCs, in control and pausing conditions, by western blot (representative of 3 biological replicates). **g.** Validation of *Mettl3*<sup>-/-#2-4</sup> ESCs, in control and pausing conditions, by western blot

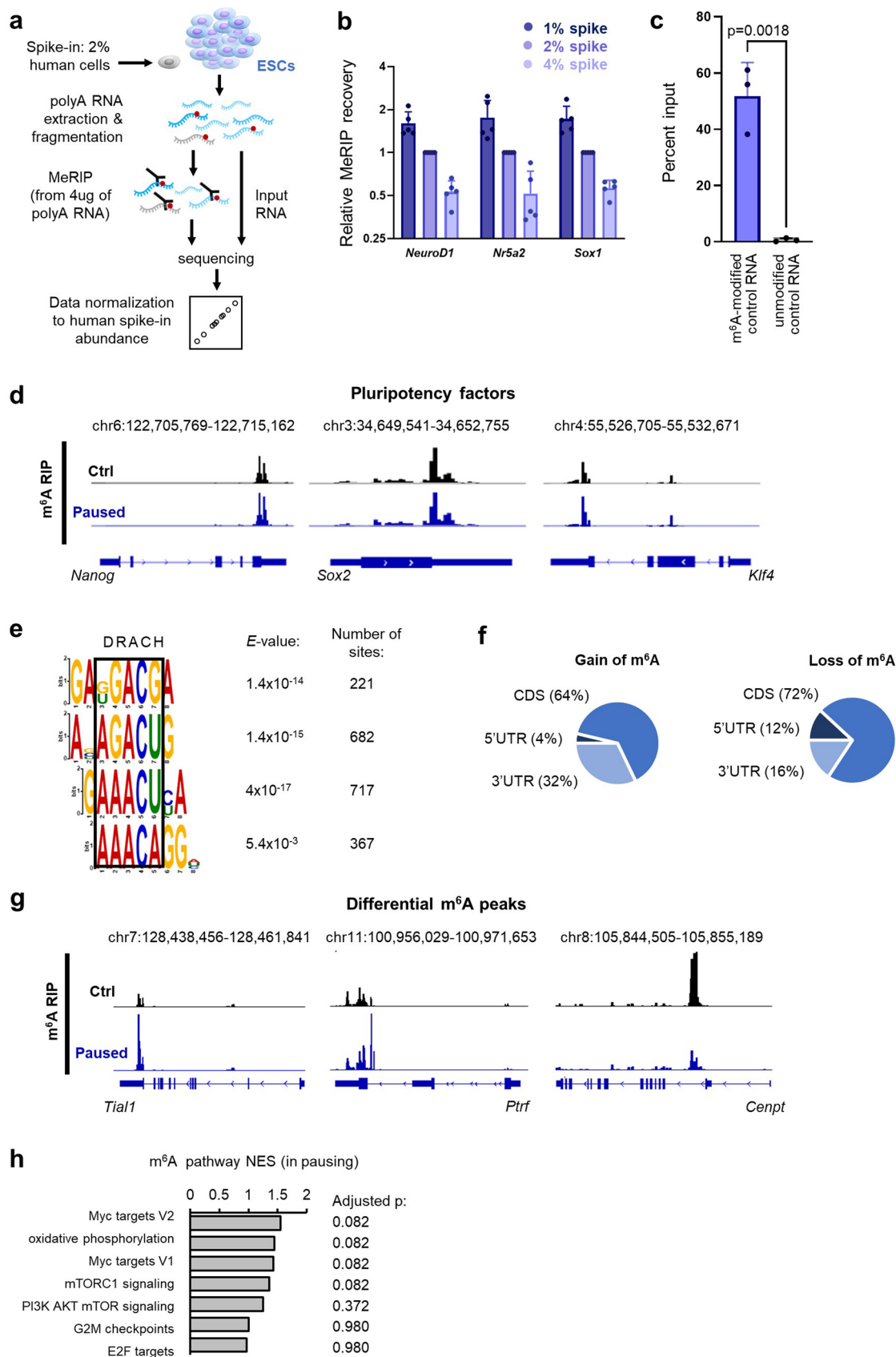
(representative of 2 biological replicates). **h.** *Mettl3*<sup>-/-#2-4</sup> ESCs also fail to suppress proliferation in paused conditions (n = 3 biological replicates). **i.** *Mettl3*-knockout mutant model in mice (*Mettl3*<sup>TCP<sup>-/-</sup>) and genotyping by PCR (left). Example of PCR genotyping of embryos resulting from *Mettl3*<sup>TCP<sup>+/-</sup> crossing, representative of all genotyping performed in this study [n(*Mettl3*<sup>TCP<sup>+/+</sup>) = 87, n(*Mettl3*<sup>TCP<sup>+/-</sup>) = 132, n(*Mettl3*<sup>TCP<sup>-/-</sup>) = 46]. +/+ : wildtype, +/- : heterozygous, -/- : knockout. **j.** Validation of *Mettl3*<sup>TCP<sup>-/-</sup> in embryos by immunofluorescence. Representative staining images are shown. Number of embryos (n) as indicated. Scale bars = 30 μm. Data are mean ± SD (**a-d**) or mean ± SEM (**h**). *P*-values (as indicated on figure) by one-way ANOVA with Dunnett's multiple comparison tests (**a-c**), two-tailed ratio paired Student's *t*-tests (**d**), and linear regression test with interaction (**h**).</sup></sup></sup></sup></sup></sup>



Extended Data Fig. 2 | See next page for caption.

**Extended Data Fig. 2 | Paused *Mettl3*<sup>-/-</sup> ESCs acquire a distinct gene expression profile.** **a.** Quantification of total RNA per cell in *Mettl3*<sup>+/+</sup><sup>#2</sup> and *Mettl3*<sup>-/-</sup><sup>#2-4</sup> ESCs, in control and paused conditions. Data are mean ± SD, n = 5 biological replicates. **b.** Decrease in nascent RNA per cell, as measured by EU incorporation with nuclear signal quantification, in wildtype ex vivo paused or hormonally diapaused blastocysts, compared to control E3.5 embryos. Number of embryos (n) as indicated. Scale bars = 30 μm. **c.** Strategy for RNA-seq with cell number-normalization using ERCC spike-in RNAs. **d.** Quantification of the number of expressed genes in *Mettl3*<sup>+/+</sup> and *Mettl3*<sup>-/-</sup> ESCs, in control and paused conditions. Expressed genes are further defined as having high expression (log<sub>2</sub> normalized reads > 5, n = 3 biological replicates). **e.** Number of differentially expressed genes (fold-change > 1.5 and adjusted *P* < 0.05) upon pausing, in *Mettl3*<sup>+/+</sup> and *Mettl3*<sup>-/-</sup> ESCs. **f.** PCA plot for all expressed genes across all samples,

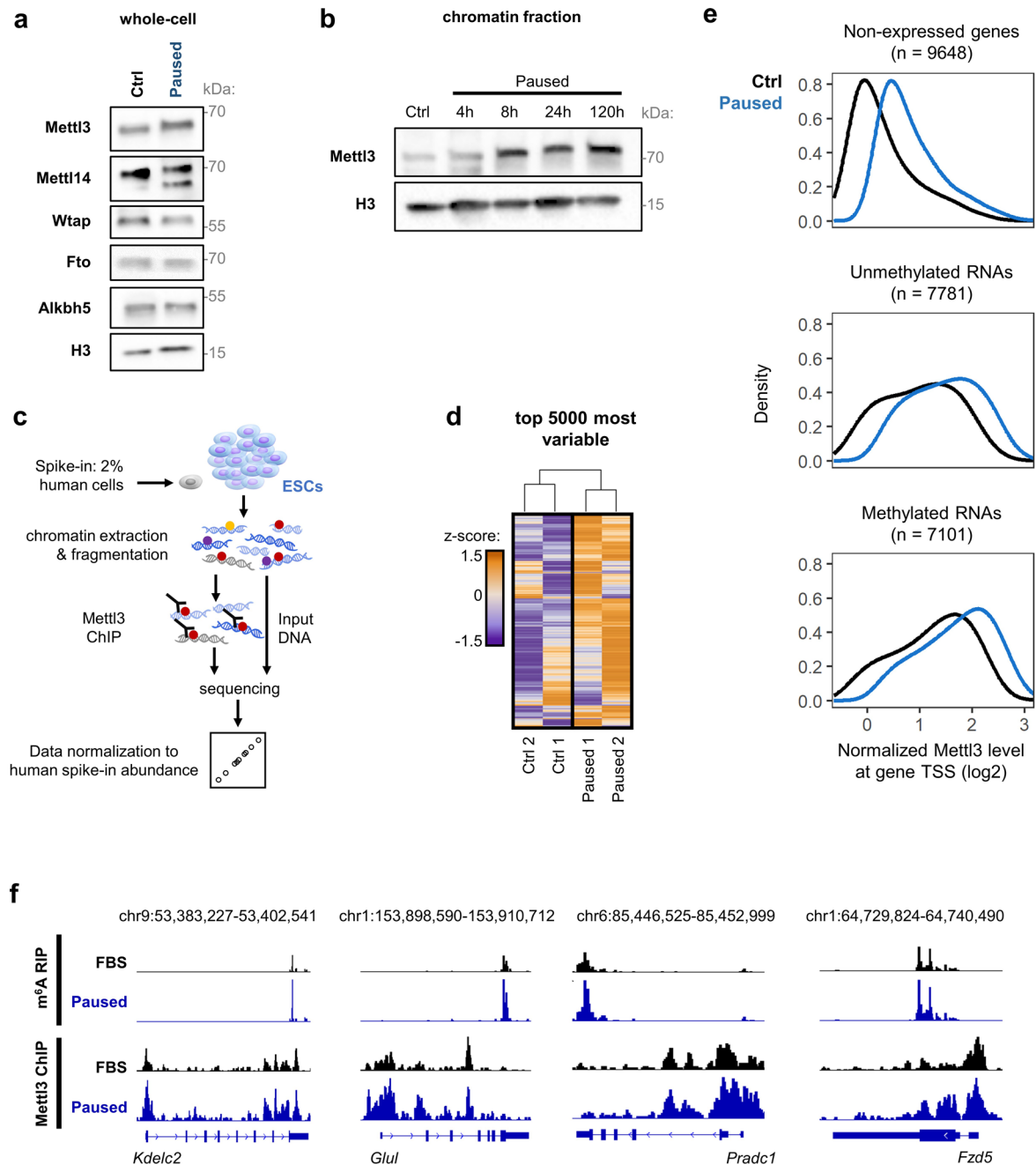
showing across PC1 that *Mettl3*<sup>+/+</sup> ESCs acquire a more divergent expression profile upon pausing than *Mettl3*<sup>-/-</sup> ESCs, relative to respective control condition. **g-h.** Gene expression changes (log<sub>2</sub> fold-changes) of gene sets selected from the 'GO biological processes' (**g**) and 'hallmarks' (**h**) collections, showing incomplete downregulation in paused *Mettl3*<sup>-/-</sup> ESCs. **i.** Western blot of total and phosphorylated mTOR, and of the downstream targets of mTORC1 (Ulk1, 4Ebp1 and S6K1) (left, representative of 4 biological replicates). Quantification of phosphorylated levels, normalized to total levels, show no significant change in paused ESCs between *Mettl3*<sup>+/+</sup> and *Mettl3*<sup>-/-</sup> (right). Data are mean ± SD (**b, d, g-i**). *P*-values (as indicated on figure) by two-way ANOVA with Dunnett's multiple comparison tests (**a, i**), one-way ANOVA with Dunnett's multiple comparison tests (**b**), two-tailed unpaired Student's *t*-tests (**d, g-h**).



Extended Data Fig. 3 | See next page for caption.

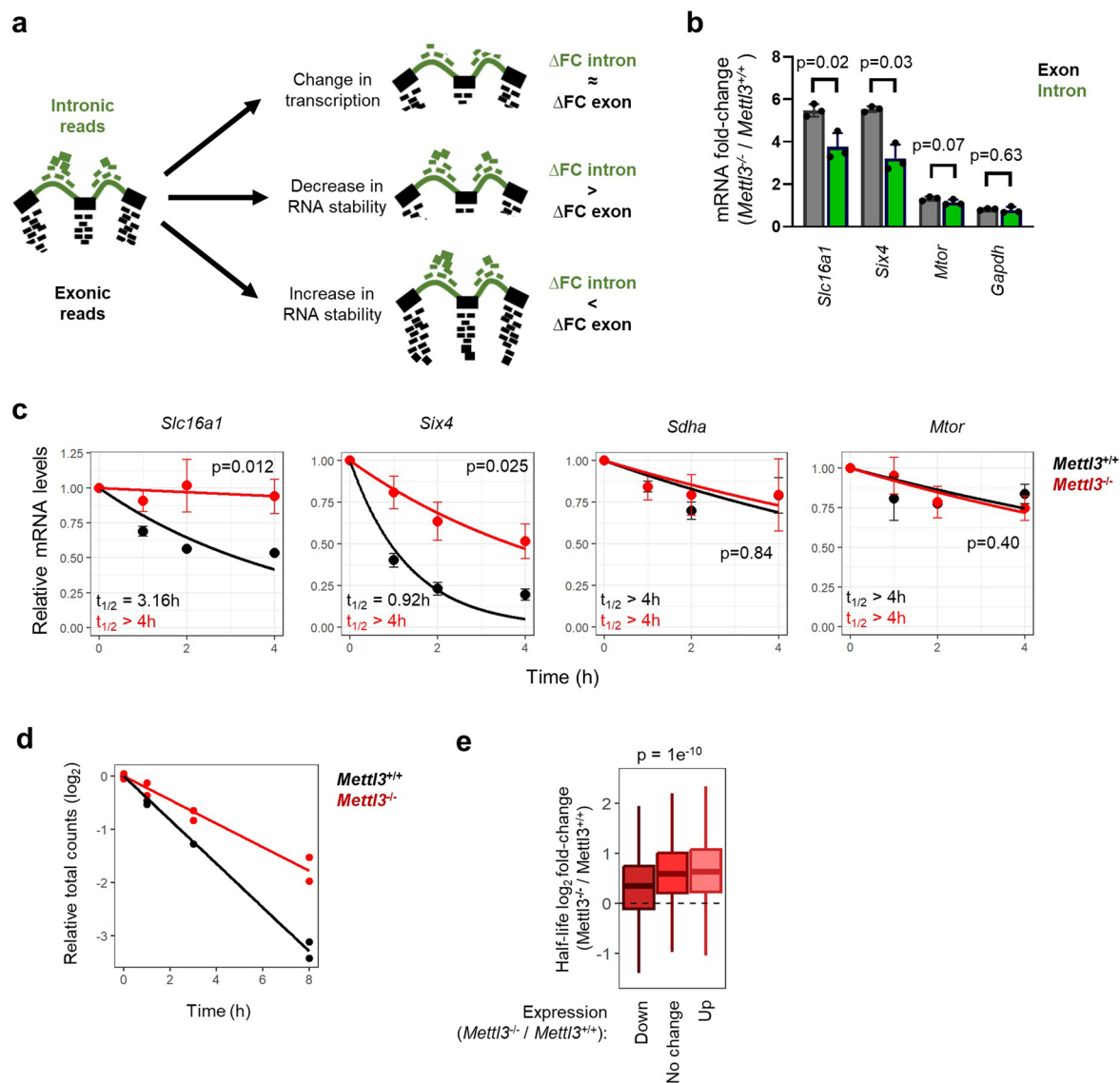
**Extended Data Fig. 3 | Mapping m<sup>6</sup>A distribution in the transcriptome of paused ESCs.** **a.** Strategy for MeRIP-seq in ESCs with cell number-normalization (CNN) using human cell spiking. **b.** Validation of the CNN strategy for the MeRIP-seq. By mixing different ratios of human cells to ESCs (1, 2 or 4%), we simulated global changes in methylation. Spiking normalization allows capture of these differences, as shown here by MeRIP-qPCR for 3 methylated mRNAs (*NeuroDL*, *Nr5a2*, *Sox1*). Data are mean  $\pm$  SD, n = 5 biological replicates with levels relative to 2% spike in each replicate. **c.** The specificity of the m<sup>6</sup>A capture was tested by spiking poly(A) RNA from ESCs with exogenous RNAs before performing MeRIP-qPCR. Data are mean  $\pm$  SD, n = 3 biological replicates. *P*-values (as indicated on figure) by two-tailed unpaired Student's *t*-tests. **d.** Examples of gene track views of MeRIP-seq, for mRNAs of pluripotency factors previously shown to be

methylated in ESCs. **e.** Motif analysis performed with DREME in a 100 bp window surrounding MeRIP peak summits identifies several motifs corresponding to the consensus 'DRACH' m<sup>6</sup>A motif (where D = A, G or U; H = A, C or U). **f.** Distribution of differential m<sup>6</sup>A peaks, according to the type of structural element within the transcript. **g.** Examples of gene track views of MeRIP-seq, for mRNAs with significant hypermethylation (*Tiall*, *Ptrf*) or hypomethylation (*Cenpt*) in pausing of ESCs. **h.** GSEA of m<sup>6</sup>A changes in paused ESCs relative to control ESCs, using the 'hallmarks' collection. No single pathway is significantly enriched based on m<sup>6</sup>A changes (representative pathways are shown). *P*-values (as indicated on figure) by two-sided pre-ranked gene set enrichment analysis with Benjamini-Hochberg FDR correction.



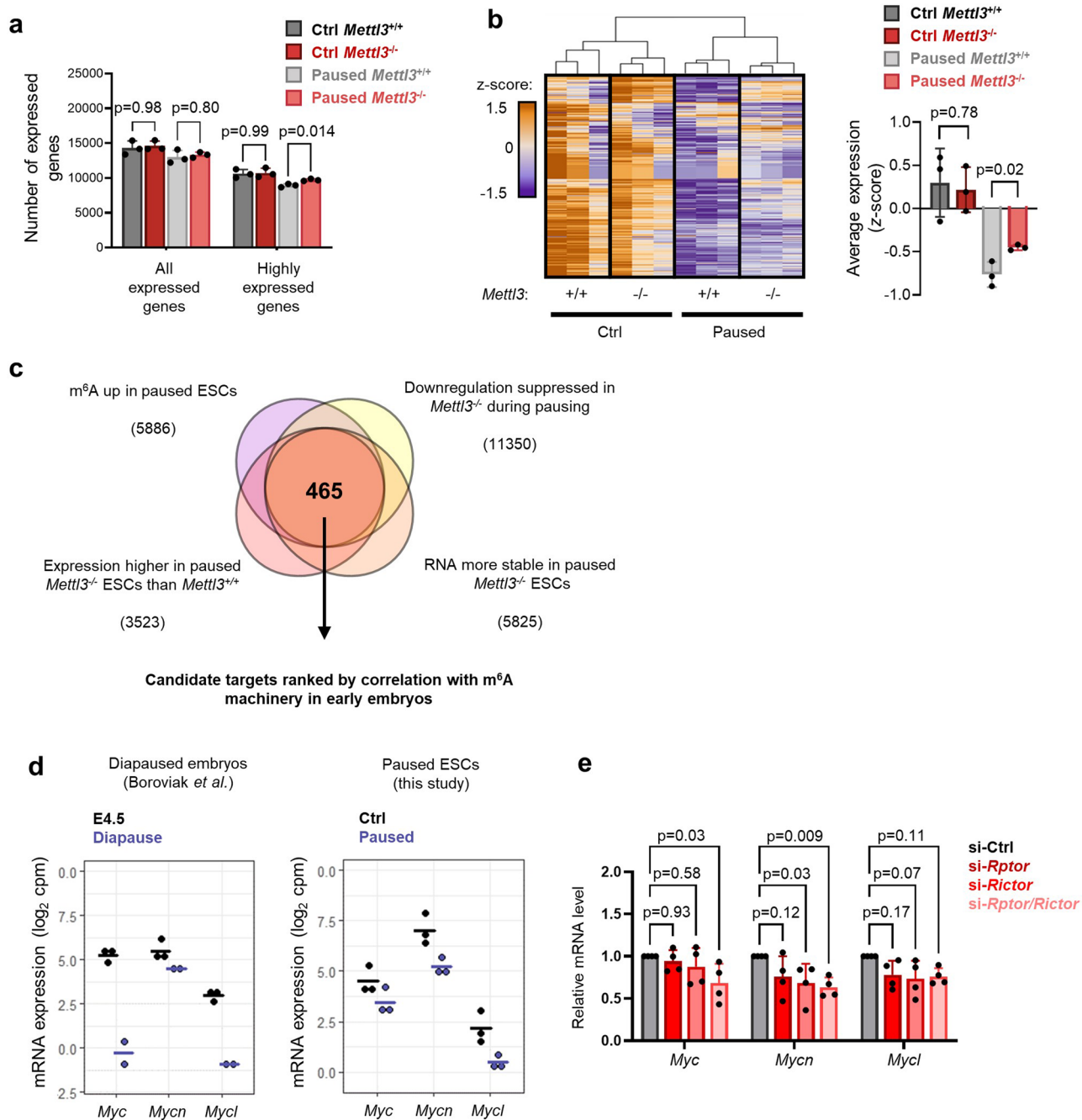
**Extended Data Fig. 4 | Mapping the chromatin distribution of Mettl3 in paused ESCs.** **a.** m<sup>6</sup>A machinery (writers Mettl3, Mettl14 and Wtap; and erasers Fto and Alkbh5) in control (Ctrl) and paused ESCs by western blot in whole cell extracts (representative of 3 biological replicates). **b.** Increase of Mettl3 levels in chromatin extracts upon induction of paused pluripotency, measured by cell number-normalized (CNN) western blot (representative of 3 biological replicates). **c.** Strategy for Mettl3 ChIP-seq in ESCs with CNN approach using human cell spiking. **d.** Heatmap of the top 5000 most variable Mettl3 peaks by ChIP-seq across all samples, showing higher levels in paused ESCs

(n = 2 biological replicates per group). **e.** Density plot of the average levels of Mettl3 binding in the TSS of all genes by ChIP-seq, separated by expression and methylation status, in control and paused ESCs. Mettl3 binding is highest in the TSS of expressed genes with a methylated transcript, and in paused ESCs. Number of genes (n) as indicated. Data as mean normalized Mettl3 level (n = 2 biological replicates per group). **f.** Examples of gene track views showing increased average levels (fold-change > 1.5) of m<sup>6</sup>A and Mettl3, by MeRIP-seq and Mettl3 ChIP-seq, respectively.



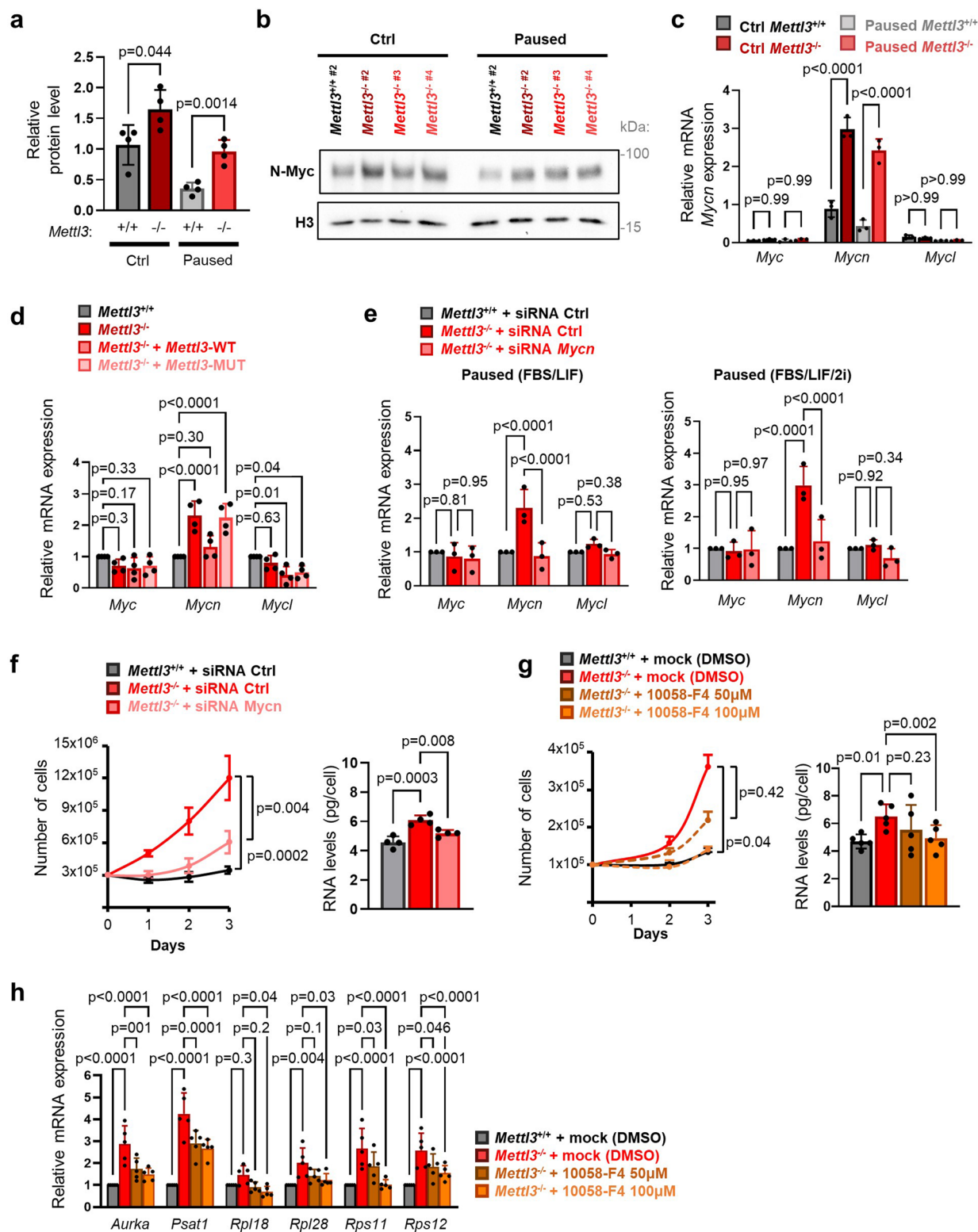
**Extended Data Fig. 5 | Capturing *Mettl3*-dependent changes in RNA stability in paused ESCs.** **a.** Strategy for RNA stability analysis based on intronic and exonic reads. **b-c.** Examples of genes with different (*Slc16a1*, *Six4*) and similar (*Mtor*, *Gapdh*) intronic and exonic mRNA fold-changes between *Mettl3*<sup>-/-</sup> and *Mettl3*<sup>+/+</sup> ESCs based on RNA-seq data (**b**) and validation of stability changes by actinomycin D stability assay (**c**).  $N = 3$  biological replicates,  $t_{1/2}$ : half-life. **d.** Linear regression of  $\log_2$  total conversion counts (relative to time 0 h), as measured by SLAM-seq, showing an increase in transcriptome stability in paused

*Mettl3*<sup>-/-</sup> ESCs. **e.** Changes in RNA expression in paused *Mettl3*<sup>-/-</sup> ESCs based on RNA-seq data (fold-change > 1.5) are associated with changes in RNA half-life in paused *Mettl3*<sup>-/-</sup> ESCs. Data are mean  $\pm$  SD (**b**) or mean  $\pm$  SEM (**c**).  $P$ -values (as indicated on figure) by two-tailed paired Student's  $t$ -tests (**b**), linear regression test with interaction (**c**) and one-way ANOVA (**e**). Boxes in the box plots define the interquartile range (IQR) split by the median, with whiskers extending to the most extreme values within  $1.5 \times$  IQR beyond the box.

**Extended Data Fig. 6 | Screening for candidate anti-pausing factors. a.**

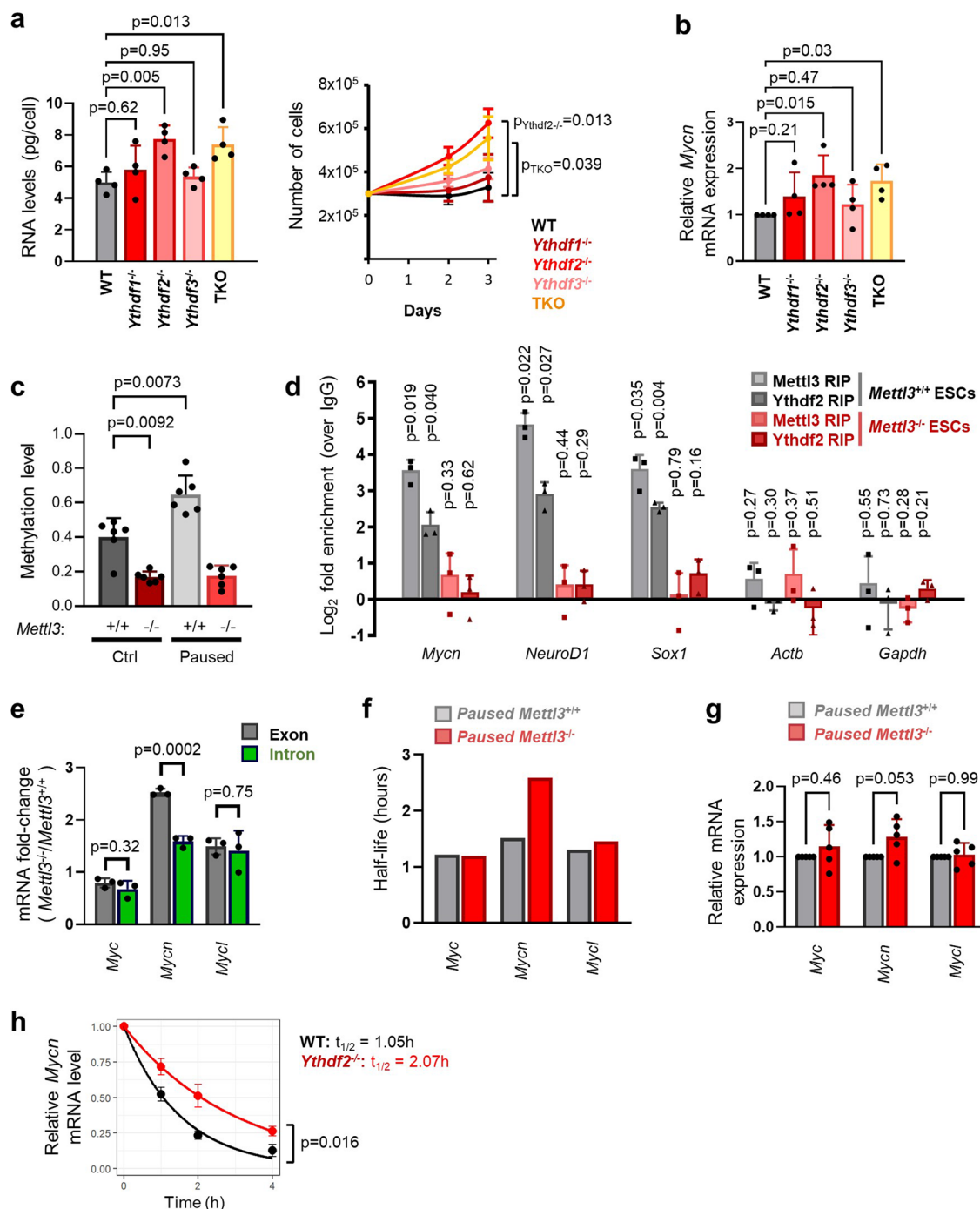
Quantification of the number of expressed genes in *Mettl3*<sup>+/+</sup> and *Mettl3*<sup>-/-</sup> ESCs based on intronic RNA-seq, in control and paused conditions. Expressed genes are further defined as having high expression ( $\log_2$  normalized reads > 5,  $n = 3$  biological replicates). **b.** Heatmap of gene expression based on intronic reads for all genes expressed in *Mettl3*<sup>+/+</sup> or *Mettl3*<sup>-/-</sup> ESCs (left) with average expression per sample (right, scored as median z-scores of all genes), showing defective hypotranscription in paused *Mettl3*<sup>-/-</sup> ESCs. **c.** Identification of putative anti-pausing factors kept in check by *m*<sup>6</sup>A methylation and thereby destabilization of their transcript in paused pluripotency, based on RNA-seq, MeRIP-seq and

SLAM-seq data in ESCs (see Methods for details). **d.** Expression levels ( $\log_2$  cpm) of the *Myc* factors in diapaused embryos (left, data from Boroviak *et al.*) and paused ESCs (right). Horizontal bars represent the mean, with 3 biological replicates per group, except for diapaused embryos which has 2 replicates. **e.** mTOR inhibition by dual knockdown of *Rptor* and *Rictor* reduces *Mycn* expression measured by RT-qPCR in ESCs in FBS/LIF/2i medium ( $n = 4$  biological replicates). Data are mean  $\pm$  SD (**a**, **b**, **e**). *P*-values (as indicated on figure) by two-way ANOVA with Tukey's multiple comparisons test (**a**), two-tailed Student's *t*-tests (**b**), and one-way ANOVA with Dunnett's multiple comparison tests (**e**).



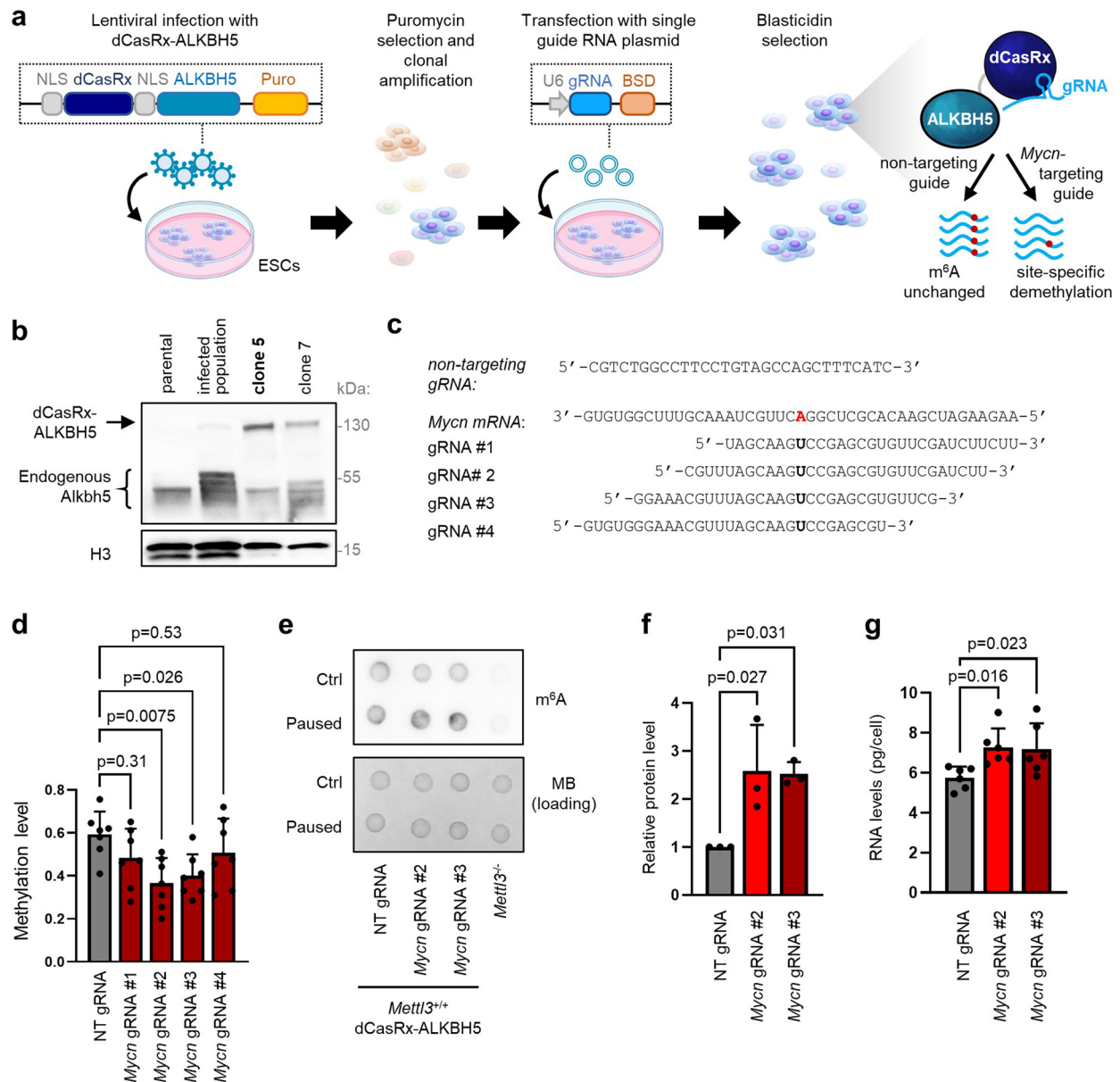
**Extended Data Fig. 7 | Regulation of Myc family members and downstream targets by Mett13 in paused pluripotency. a.** Quantification of N-Myc protein levels, showing increased expression in *Mett13*<sup>-/-</sup> ESCs, as shown in Fig. 5c. N = 4 biological replicates. **b.** Representative western blot of N-Myc protein levels, showing increased expression in *Mett13*<sup>-/-</sup> ESCs. N = 2 biological replicates. **c.** Increased expression of N-Myc in *Mett13*<sup>-/-</sup> ESCs grown in FBS/LIF/2i (compared to *Mett13*<sup>+/+</sup> ESCs) measured by RT-qPCR (n = 3 biological replicates). Levels are normalized to control *Mett13*<sup>+/+</sup> ESCs grown in FBS/LIF, as shown in Fig. 5b. **d.** *Mycn* expression in *Mett13*<sup>-/-</sup> ESCs is restored to levels comparable to *Mett13*<sup>+/+</sup> ESCs by transfecting a catalytically active form of Mett13, and not its inactive mutant form (RT-qPCR, n = 4 biological replicates). **e.** Validation of *Mycn* knockdown by

RT-qPCR in paused ESCs grown in FBS/LIF (left) or FBS/LIF/2i (right). **f-g.** Blocking of Myc signaling by *Mycn* knockdown (**e**, in FBS/LIF/2i) or chemical inhibitor 10058-F4 (**f**, in FBS/LIF) partially restores the pausing phenotype in paused *Mett13*<sup>-/-</sup> ESCs in terms of cell proliferation (left, n = 3 biological replicates) and total RNA levels per cell (right, n = 4 and 5 biological replicates). **h.** Treatment with 10058-F4 partially restores the expression of Myc target genes in paused *Mett13*<sup>-/-</sup> ESCs (RT-qPCR, n = 5 biological replicates). Data are mean ± SD (**a**, **c-h**), or mean ± SEM (g left). P-values (as indicated on figure) by two-tailed unpaired Student's t-tests (**a**, **d**, **f**), by two-way ANOVA with Tukey's multiple comparisons test (**c**) or Dunnett's multiple comparison tests (**d-e**), one-way ANOVA with Dunnett's multiple comparison tests (**f-g**).

**Extended Data Fig. 8 | m<sup>6</sup>A-dependent regulation of Mycn mRNA stability.**

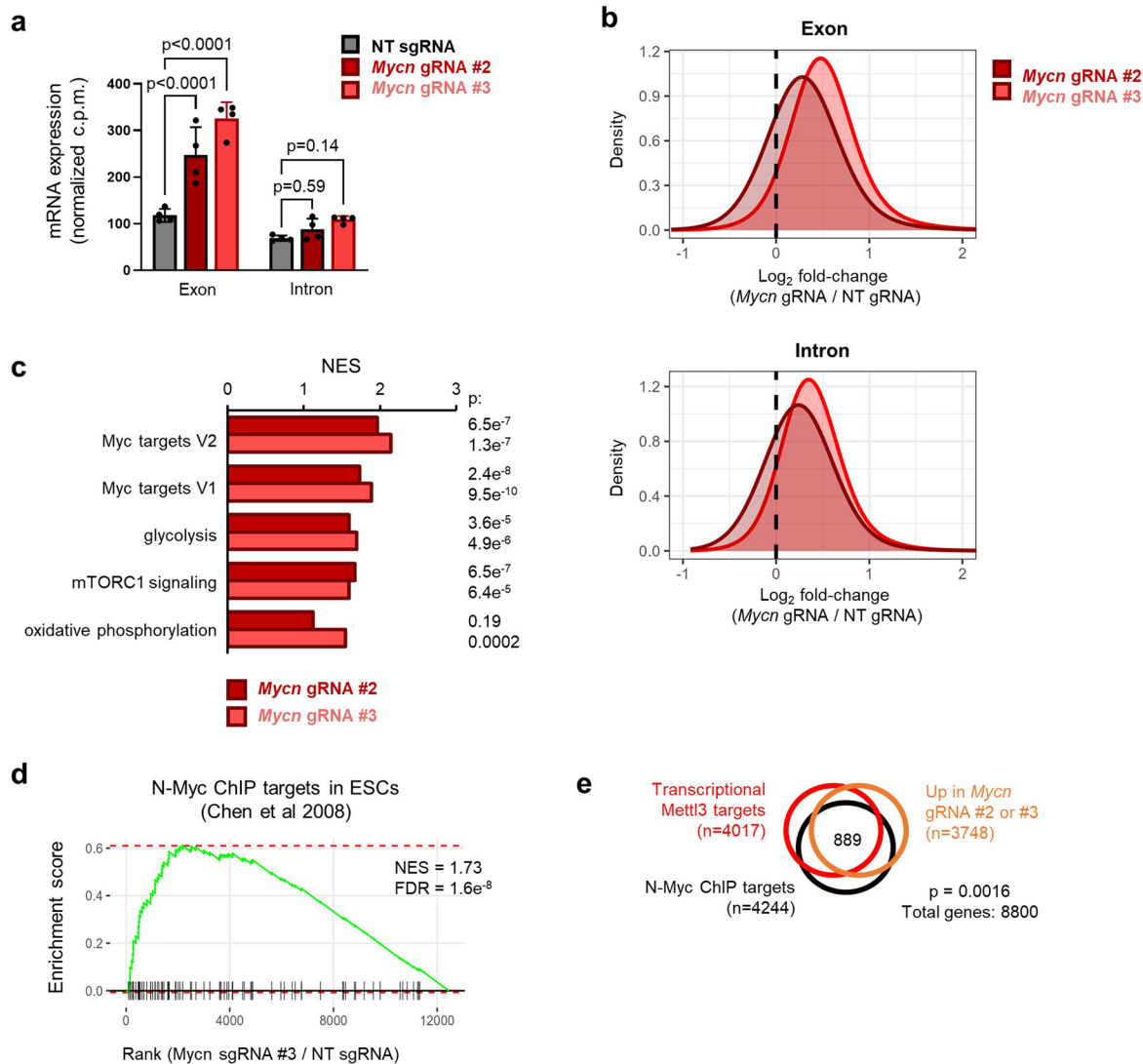
**a.** Knockout of *Ythdf2* and triple knockout of *Ythdf1-3* (TKO) phenocopy the knockout of *Mettl3* in paused ESCs, with increased total RNA levels per cell (left,  $n = 4$  biological replicates) and proliferation (right,  $n = 4$  biological replicates) compared to wildtype (WT) ESCs. **b.** Increased expression of N-Myc in paused *Ythdf2<sup>-/-</sup>* and TKO ESCs measured by RT-qPCR ( $n = 4$  biological replicates, relative to paused WT). **c.** Validation of m<sup>6</sup>A changes in *Mettl3<sup>+/+</sup>* and *Mettl3<sup>-/-</sup>* ESCs by m<sup>6</sup>A-qPCR ( $n = 6$  biological replicates). **d.** *Mettl3* and *Ythdf2* binding of the *Mycn* transcript, measured by RIP-qPCR in 3 biological replicates. *NeuroD1* and *Sox2* were used as positive controls, and *Actb* and *Gapdh* were used as negative controls. **e-f.** *Mycn* is the only Myc family member regulated at the RNA stability

level by *Mettl3*, as evidenced by analysis of exonic and intronic mRNA fold-changes (left,  $n = 3$  biological replicates per group) and SLAM-seq analysis of RNA half-life (right, with half-lives derived from 2 independent time courses). **g.** Nascent RNA capture by EU incorporation shows minimal changes in nascent transcription for Myc factors in *Mettl3<sup>-/-</sup>* ESCs ( $n = 5$  biological replicates). **h.** Increased *Mycn* mRNA stability in paused *Ythdf2<sup>-/-</sup>* ESCs compared to paused *Mettl3<sup>+/+</sup>* ESCs, as measured by an actinomycin D stability assay ( $n = 3$  biological replicates).  $t_{1/2}$ : half-life. Data are mean  $\pm$  SD (**a-e, g**) or mean  $\pm$  SEM (**h**). *P*-values (as indicated on figure) by one-way ANOVA with Dunnett's multiple comparison tests (**a-c**), two-tailed Student's *t*-tests (**d-e**), two-way ANOVA with Dunnett's multiple comparison tests (**g**), and linear regression test with interaction (**h**).



**Extended Data Fig. 9 | Targeted m<sup>6</sup>A demethylation controls expression of *Mycn* in paused ESCs.** **a.** Model of lentiviral dCasRx epitranscriptomic editor with the m<sup>6</sup>A demethylase ALKBH5 and single guide RNA. **b.** Validation of the expression of the dCasRx-ALKBH5 fusion by western blot in parental (non-infected) ESCs, infected ESCs, and 2 infected clones. Clone 5 was used for all experiments (representative of 2 biological replicates). **c.** Guide RNAs (gRNAs) transfected for non-targeting control and *Mycn*-targeting conditions. **d.** Changes in m<sup>6</sup>A using the dCasRx-ALKBH5 editor in paused ESCs. Guides #2 and #3 significantly reduce m<sup>6</sup>A in *Mycn* transcripts, as measured by m<sup>6</sup>A-qPCR, and were selected for all subsequent experiments. N = 7 biological replicates.

NT: non-targeting. **e.** Dot blot showing that the global increase of m<sup>6</sup>A in paused ESCs is not affected by the dCasRx-ALKBH5 editor, with *Mettl3*<sup>-/-</sup> ESCs as negative control. Representative of 3 biological replicates. MB: methylene blue. **f.** Quantification of N-Myc protein levels, showing increased expression with the dCasRx-ALKBH5 editor targeting *Mycn* in paused ESCs, with representative blot shown in Fig. 6e. N = 3 biological replicates. **g.** Demethylation of *Mycn* increases the total RNA levels per cell in paused ESCs (n = 6 biological replicates). Data are mean ± SD (**d**, **f-g**) and P-values (as indicated on figure) by one-way ANOVA with Dunnett's multiple comparison tests (**d**, **f-g**).



**Extended Data Fig. 10 | Transcriptional changes by RNA-seq upon m<sup>6</sup>A demethylation of *Mycn* in paused ESCs.** **a.** *Mycn* expression is increased following targeting with the m<sup>6</sup>A demethylase ALKBH5 based on exonic reads, but not intronic reads, which is consistent with post-transcriptional regulation (n = 4 biological replicates per condition). **b.** A global increase in transcripts levels is measured following *Mycn* mRNA demethylation using both exonic and intronic reads, which is consistent with globally elevated nascent transcription. **c.** Representative pathways of the GSEA of gene expression changes upon demethylation of *Mycn* mRNA in paused ESCs using the ‘hallmarks’ collection.

**d-e.** Genes upregulated upon demethylation of *Mycn* mRNA are enriched for N-Myc targets, as identified in ESCs by ChIP by Chen *et al.*<sup>36</sup>. GSEA using a random set of 100 N-Myc targets (c). Venn diagram showing a significant overlap between genes upregulated in paused *Mettl3*<sup>-/-</sup> ESCs, genes upregulated following *Mycn* demethylation, and N-Myc ChIP targets. Data are mean ± SD (a). P-values (as indicated on figure) by two-way ANOVA with Dunnett’s multiple comparison tests (a), two-sided pre-ranked gene set enrichment analysis with Benjamini-Hochberg FDR correction (c, d), and one-sided simulation using hypergeometric distributions (e).